Stable Spin Coated SnO_2 Thin Film with MTMS and TEOS

By

NANDHINI M

(Reg No. 21PPH011)

Supervisor

Dr.J.Shanthi

Department of physics

A Thesis submitted to

Avinashilingam Institute for Home Science and Higher Education for Women, Coimbatore-641043

In Partial Fulfilment of the requirements for the Degree of

MASTER OF SCIENCE IN PHYSICS

MAY 2023

Stable Spin Coated SnO_2 Thin Film with MTMS and TEOS

By

NANDHINI M

(Reg No. 21PPH011)

Supervisor

Dr.J.Shanthi

Department of physics

A Thesis submitted to

Avinashilingam Institute for Home Science and Higher Education for Women, Coimbatore-641043

In Partial Fulfilment of the requirements for the Degree of

MASTER OF SCIENCE IN PHYSICS

MAY 2023

CERTIFIED AS A BONAFIDE RESEARCH WORK

11/05/23

Signature of Head of the Department

Dr. J. SHANTHI, M.Sc., M.Phil., Ph.D.,
Professor and Head
Department of Physics
Avinashilingam Institute for Home Science
and Higher Education For Women
Coimbatore - 641 043.

11/05/23

Signature of the Supervisor

Dr. J. SHANTHI, M.Sc., M.Phil., Ph.D.,
Professor and Head
Department of Physics
Avinashilingam Institute for Home Science
and Higher Education For Women
Coimbatore - 641 043.

ACKNOWLEDGEMENT

ACKNOWLEDGEMENT

I owe my sincere gratitude to **My Parents** for showering their generous blessings upon me in all my endeavors and for their constant support in all my steps.

I express my deep sense of reverential gratitude to **Dr. S.P. Thyagarajan**, Chancellor, Avinashilingam Institute for Home Science and Higher Education for Women, Coimbatore, for all the good wishes towards the successful completion of the study.

I extend my thanks to **Dr. (Tmt.) Bharathi Harishankar**, Ph.D., FRSA, Vice Chancellor, Avinashilingam Institute for Home Science and Higher Education for Women, Coimbatore, for her constant motivation and encouragement towards our academic performance.

I record my deep sense of gratitude and indebtedness to **Dr. (Tmt.) S. Kowsalya**, MSc., MPhil., Ph.D., Registrar, Avinashilingam Institute for Home Science and Higher Education for Women, Coimbatore, for providing adequate help for my study.

I also wish to express my gratitude to **Dr. (Tmt.) G. Padmavathi**, MSc.,MPhil.,Ph.D., Dean, School of Physical Sciences & Computational Sciences, Avinashilingam Institute for Home Science and Higher Education for Women, Coimbatore, for her encouragement and generous help which was of great value.

I express my sincere reverence and gratitude to my guide **Dr. (Tmt.) J. Shanthi**, MSc., MPhil., Ph.D., Professor and Head, Department of Physics, Avinashilingam Institute for Home Science and Higher Education for Women, Coimbatore, for her guidance, motivation, valuable advice, untiring support, timely suggestions, constant encouragement, inspiration throughout the study and holding me strong in all places I flatered.

I express my gratitude to **Ms. N. R. Chandralekha**, Research Scholar, Department of Physics, Avinashilingam Institute for Home Science and Higher Education for Women, Coimbatore, for her kind support, encouragement and valuable help in the completion of my project.

I would like to thank all the teaching and non – teaching staff of the Department of Physics, Avinashilingam Institute for Home Science and Higher Education for Women, Coimbatore, and my friends for their support and cooperation during the time course of my work.

M. NANDHINI

List of Contents

List of Tables

List of figures

CONSTANTS AND SYMBOLS

γ_{SV} - interfacial tensions between the solid–vapor phase

γ_{SL} - interfacial tensions between the solid–liquid phase

γ_{LV} - interfacial tensions between the liquid–vapor phase

Θw - Wenzel's CA on the rough surface

Θr - Young's CA on the smooth surface

Θ_{CB} - Cassie – Baxter CA on the rough surface

t - Thickness of the film

w - Weight of the film on the substrate

ρ - density of the material

A -Area of the substrate

ABBREVATION

CA - Contact angle

TEOS - Tetraethoxysilane

MTMS -Methyltrimethoxysilane

HCl - Hydrochloric acid

PVD - Physical vapour deposition

CVD - chemical vapour deposition

FTIR - Fourier Transform infrared spectroscopy

XRD -X - ray Diffraction

Chapter – I

Introduction

CHAPTER – I

1.1 Introduction

In a natural environment, the accumulation of dust particles or other contaminants on glass surface causes a serious problem, which requires high maintenance cost to make it clean. There are many glass cleaning methods and technologies, such as manual cleaning, automatic cleaning, laser cleaning etc. All of these methods are expensive and consume large amount of cleaning agents, which also causes secondary pollution **(Gao et al., 2021)**. Self-cleaning coating on the glass surface is proposed as one of the possible solutions to maintain the durability of the material against dust accumulation. Many surfaces in nature exhibit self - cleaning properties. The wings of butterflies and leaves of plants such as cabbage and lotus are few examples. The requirements for this type of coating have adopted from distinctive structural and functional properties of lotus leaves. It has been found that the self - cleaning property of lotus leaf is mainly due to its structured surface roughness in combination with low surface energy of biological epicuticular wax crystals. Hence, lotus leaf has a static contact angle $\geq 150^{\circ}$ and sliding angle $<10^{\circ}$, this surface known as super hydrophobic surface **(Pratiwi et al., 2020).** This technology received a great deal of attention during the late 20^{th} century and now numerous research works are going on around the world to develop highly efficient and durable self - cleaning coating surfaces with enhanced optical quality **(Chem et al., 2011).**

1.2 Self – cleaning effect

The self-cleaning phenomenon is related to the surface contact angle. It is the angle formed at the three phase boundary (solid/ liquid/vapour) between the surfaces of the liquid drop to the surface of the solid. Self – cleaning property can be achieved either by super – hydrophobicity or super hydrophilicity, which repel and stick the water respectively, results in a water contact angle greater than 150° and smaller than 10° **(Swathi et al., 2021)**. Self-cleaning surfaces can be cleaned simply by rinsing with water, can be potentially applied in many areas. As exterior surfaces, such materials will be cleaned just with regular rain significantly reducing maintenance costs **(Parkin & Palgrave, 2005).** Self-cleaning glasses can be fabricated by coating with thin films, which give good optical transparency on the glass substrates. Various methods have been developed to prepare artificial self – cleaning coatings. However, most of these techniques involve high cost and complexity procedures. But, the wet-chemical methods such as sol-gel method combining with dip or spin coating technique are well known and more flexible in approach to form a cost-efficient thin film coatings **(Qian et al., 2014)**. High

transmission and self - cleaning properties of thin film can be significantly used in solar panels. Large number of studies has been reported on the various roles of dust deposition on solar panel efficiency.

1.3 Theory of Wettability

Wetting is a study of how liquids make contact with the solid, such interaction involves multiple surfaces which come together at three phase line, the result of such interaction are characterized by contact angle. The sessile droplet contact angle (CA) has been widely used as an indicator of the wettability characteristics. The Contact angle is evaluated as an angle between the tangent of three-phase contact line. Contact angle is directly proportional to surface energy i.e., surface energy decreases with decrease in contact angle. Based on the conventional wettability criteria, systems with static CA of less than 90° are regarded as hydrophilic (water-attracting) whereas those with CA greater than 90° are hydrophobic (water-repelling). In fact, the idea of wetting characterization based on the CA originates from the work of Thomas Young more than 200 years ago **(Kung et al., 2019)**.

Wetting of a surface is characterized by two distinct states i,e., complete wetting and complete non-wetting. Complete wetting is characterized by a contact angle of 0° and that of non-wetting by a contact angle 180°. All intermediate states of wetting with contact angles between 0° and 180° are possible. Reversible wettability of these surfaces leading to self-cleaning surfaces. Self-cleaning surfaces have drawn considerable interest from perspectives of both fundamental research and applications. They find applications in diverse fields from daily life to the industry including self-cleaning exterior construction materials, interior furnishing materials, road construction materials, solar cells, car mirrors, textiles, utensils, roof tiles, etc **(Krishna et al., 2013)**. The wetting behaviour of a liquid on a solid substrate is determined by the difference between the cohesive interactions holding the liquid. The states of wettability is tabulated in Table 1.1.

Table 1.1 States of Wettability

Contact angle	Degree of wetting
$\theta = 0^{\circ}$	Perfect wetting
$0 < \theta < 90^{\circ}$	High wettability
$90^{\circ} \leq \theta < 180^{\circ}$	Low wettability
$\theta = 180^{\circ}$	Perfect non- wetting

1.3.1 Young's equation

An ideal solid surface is defined as topographically smooth, rigid, chemically homogeneous, insoluble, and non - reactive. The homogeneity of the surface results in uniform surface energy and such ideal surface has a single unique CA value. The CA on such surfaces can be described using the Young's equation through the Young's contact angle (YCA).

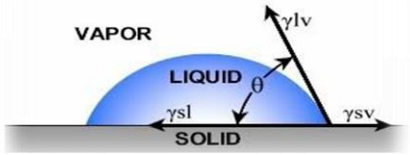

Fig 1.1 Young's regime

In the nineteenth century, Thomas Young modelled the static contact angle of a droplet on a smooth surface. He stated that interplay between the surface free energies of the solid–liquid, solid–gas and liquid–gas boundaries determined the water contact angle. If the wetted surface is more energetically favourable than the dry surface, the static contact angle will be less than 90° and the surface is termed hydrophilic. If the dry surface is more favourable, then the surface is hydrophobic, and its static contact angle will be greater than 90°.

The Young's equation formulated based on the force balance at the interface of all three phases (solid, liquid, and vapour), it is one of the most well-known models used to quantify the solid surface energy using the macroscopic CA. Young's equation through the Young's contact angle (YCA) is written as,

$$\mathbf{Cos\ \Theta_y = (\gamma_{SV} - \gamma_{SL}) / \gamma_{LV}} \qquad \textbf{- - - - - - - - - - - (1.1)}$$

In the above representation, γ_{SV}, γ_{SL}, and γ_{LV} are interfacial tensions between the solid–vapor phase, solid–liquid phase, and liquid–vapor phase, respectively. For smooth surfaces the contact angle Θ lies in the range $0° < \Theta < 90°$ and has well wetting property and fluid will spread over a large area on the surface, the surface is termed as hydrophilic **(Aishwarya et al., 2019)**.

1.3.2 Wenzel state

Water repellency has received much attention in the development of self-cleaning materials, and it has been studied in both natural and artificial systems **(Yamamoto et al., 2015)**.

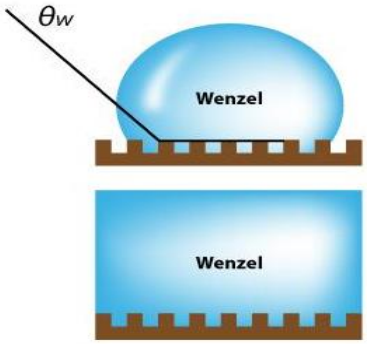

Fig 1.2 Wenzel regime

The wetting properties of a material are governed by its chemical composition and surface geometrical structure. Depending on the interplay between these two factors, wetting of rough solid surfaces can be classified into two general categories; one involves complete or homogeneous wetting of the entire area by the liquid i,e., no vapour or air is trapped between the liquid and solid surface, such condition are said to constitute Wenzel wetting or Wenzel state. The complete wetting state on the rough surface is written as,

$$\mathbf{Cos\ \Theta w = r\ Cos\ \Theta r} \qquad \textbf{- - - - - - - - - - - (1.2)}$$

Where, Θw is the Wenzel's CA on the rough surface, and r is the surface roughness factor, and Θr is the Young's CA on the smooth surface of the same material. In this equation r is always greater than unity. Therefore, the surface roughness enhances wettability of the solid surface.

1.3.3 Cassie - baxter state

When the liquid makes only partial contact with solid and balanced on the elevated regions of the solid, i,e., the liquids is in contact with both solid regions and pockets of vapour or air forming composite interface, this heterogeneous wetting condition is said to constitute cassie - baxter wetting or cassie - baxter state. As a result of intrusion of air in the rough structure, a water molecule is not able to displace the air. The apparent-contact angle (θCB) in this case is given by the Cassie-Baxter's equation. Partial wetting of a rough surface can be evaluated by Cassie – Baxter equation

$$\mathbf{Cos\ \Theta_{CB} = r_f f\ Cos\ \Theta r + f - 1} \qquad \textbf{- - - - - - - - - - - (1.3)}$$

where, Θ_{CB} is the Cassie – Baxter CA on the rough surface, r_f is the actual wetted area divided by the projected wetted area of the surface, and f is the fraction of the projected area of the surface that is wetted by the liquid.

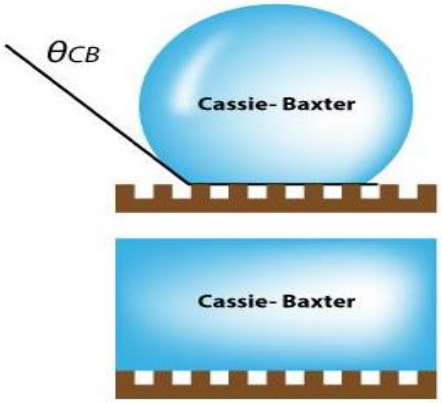

Fig 1.3 Cassie - baxter regime

Both the models explain how surface roughness increases with an increase in the contact angle. The water repelling ability of various materials have shown great influence on various applications such as self-cleaning, anti-ageing, water-oil separation, water proof textiles, etc **(Aishwarya et al., 2019).**

The pictorial representations of Wenzel and Cassie-Baxter equations are given in Figure 1.3. In Wenzel's model, the liquid droplet keeps contact with the solid surface at all points whereas in Cassie state the liquid sits only across surface protrusions, thus resulting in a droplet suspended on a composite solid and vapor phase. In general, Wenzel's model deals with the homogeneous surfaces whereas Cassie-Baxter's model was found to be functional for heterogeneous surfaces. These models have been used, traditionally, to explain all wettability behavior **(Krishna et al., 2013).**

1.4 Thin film technology

A thin film is a layer of material ranging from fractions of a nano meter (monolayer) to several micro meters in thickness. The controlled synthesis of materials as thin films (a process referred to as deposition) is a fundamental step in many applications. Thin film deposition is the process of creating and depositing thin film coatings onto the substrate material. These coatings can be made of different materials like metals oxides, polymer, silanes etc. Thin film coatings also have many different characteristics which are leveraged to alter or improve performance such as transparency, durability, scratch resistant, electrical and optical conductivity. Thin film deposition is an important manufacturing step in the production of many opto-electronic, medical devices and products including semiconductor lasers, fiber lasers, LED displays, optical filters, etc. The required properties and versatility can be obtained

by choosing proper method of thin films deposition. Thin film deposition methods can be broadly classified as;

- Physical Vapor Deposition (PVD)
- Chemical Vapor Deposition (CVD)

Physical method covers the deposition techniques which depend on the evaporation or discharge of the material from a source, i.e. evaporation or sputtering, whereas chemical methods depend on physical properties and solid films are formed on the substrate by chemical reaction of vapor phase chemicals that contain the required constituents.

The properties of thin films depend on the method of deposition. The property of thin film generally varies from the values of the physical parameters of the materials in bulk form is given. Films may be not fully dense, under stress, quasi two dimensional, different defect structures from the bulk material, Strongly influenced by surface and interface effects.

1.5 Self-cleaning surfaces

When water hits the surface, it can behave in several different ways. It can either spread on the surface completely, roll off the surfaced, or stay as droplet. Depending on the shape of the droplet, more precisely the angle that the water drop takes as it sits on the surfaces, the surface termed as hydrophobic , hydrophilic, super hydrophobic and super hydrophilic. These surfaces clean themselves through the action of water, the former by rolling droplets and the latter by sheeting water that carries away dirt.

1.5.1 Hydrophilic surface

The most recognizable definitions in surface science are hydrophobicity and hydrophilicity. In the Greek words, hydro means water, philicity means affinity. Hydrophilic surface has a strong affinity to water. Hydrophilic surfaces have the ability to absorb and hold water. A hydrophilic surface can thus be considered as water-loving which makes a water droplet spread on it. Properties of hydrophilic surface are needed in many different applications ranging from biomedical devices to marine engineering. The degree of hydrophilicity of the substance can be measured by measuring the contact angle between the liquid and solid phases. Contact angle measurement is a major parameter to quantify the hydrophilicity of a substance, which is further indicative of wettability. The contact angle (θ) is the angle between the surface and the edge of the droplet. A hydrophilic surface has a contact angle (θ) $<90^{\circ}$ and above 10°, thus it possess good wettability.

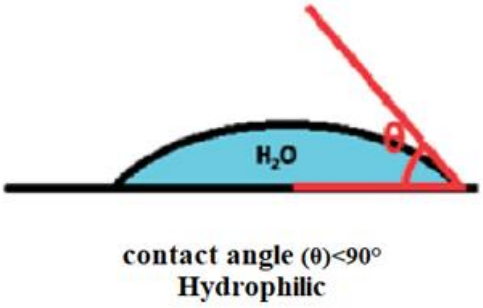

Fig 1.4 Hydrophilic surface

1.5.2 Super-hydrophilic surface

Super-hydrophilic surfaces have drawn considerable interest in recent years due to extensive application in antifogging and self-cleaning surfaces. The self-cleaning, transparent super hydrophilic coatings have high potential applications as window glasses, automobile glasses, mirrors and so on. Super hydrophilic surface spreads water droplets to form a film throughout itself, thereby, allowing light waves to pass through. Metal oxides such as TiO_2, SnO_2 and ZnO have been studied due to photoinduced superhydrophilicity under UV irradiation **(Paul & Purkayastha, 2017).** In general, super hydrophilic coating on glass substrate possesses water contact angle (WCA) below 10° and contains high self-cleaning properties in outdoor environment as compared to uncoated glass. The self-cleaning property of thin films was evaluated by measuring the static contact angle between de-ionized water and thin films with and without UV irradiation. Water droplets were placed at 3 different positions for one sample and the averaged value was adopted as the contact angle **(Sangchay & Rattanakool, 2014).**

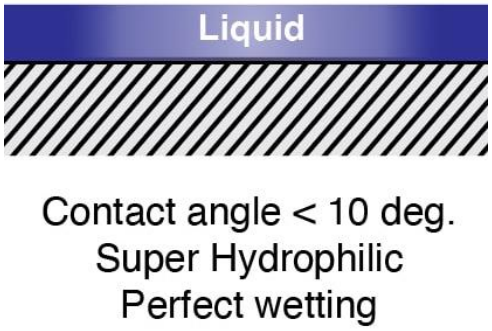

Fig 1.5 Superhydrophilic surface

1.5.3 Hydrophobic surface

The water repellent behaviour plays an important role in many applications such as anti-adhesion, self - cleaning, anti - biofouling, corrosion inhibition, and drag reduction. Water repellency is dominated by the solid surface chemical properties and surface morphology. The combination of a low surface energy and rough surface determines the hydrophobic properties of the thin film **(Widati et al., 2017)**.

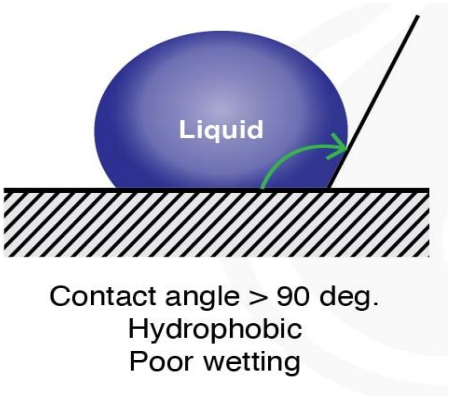

Fig 1.6 Hydrophobic surface

Hydrophobic surfaces shows extremely low wettability and Hydrophobic coatings on glass substrate possesses water contact angle (WCA) above 90° and contains high self-cleaning properties. The nanostructures of this surface can enhance the contact angle (CA) higher than 90°, so the Water droplets that hit the surface would quickly roll off, carrying dust and other particles with them. When a droplet rolls, an hysteresis develops in the contact angles at the advancing and receding three-phase interface between solid, liquid and gas. Theory as to how this hysteresis varies with the chemical and topological properties of the surface is still being developed, but ideally hysteresis should be as close as possible to zero if drops are to roll easily, at low surface inclination angles **(Parkin & Palgrave, 2005).** Because droplets tend to roll only on surfaces with very high static contact angle. Nevertheless, most studies regarding hydrophobic surfaces have focused mostly on enhancing the non-wetting property of the thin film **(G. He et al., 2011).** From a viewpoint of surface roughness, hydrophobicity is competitive with its transparency because surface roughness becomes a scattering source of light. Hence, to fulfil both hydrophobicity and transparency, precise control of roughness is necessary **(Nakajima et al., 2000).**

1.5.4 Super – hydrophobic surface

We often see spherical water droplets on floating lotus leaves. This phenomenon is due to innumerable fine projections coated with water-repellent wax on the leaf. A surface with such excellent hydrophobicity has a high contact angle for water, and a surface whose water contact angle is greater than 150° is commonly called a super hydrophobic surface.

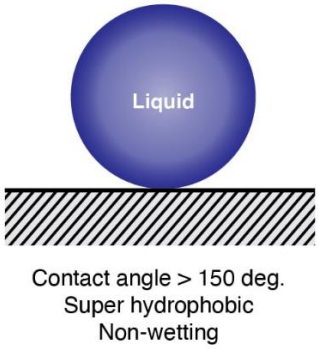

Fig 1.7 Superhydrophobic surface

Superhydrophobicity results when the normal hydrophobicity of a smooth substrate is amplified by roughness. In addition, for practical applications, the surfaces should also exhibit low contact angle hysteresis along with self - cleaning properties. The lotus effect (named after the lotus plant, Nelumbo nucifera), which describes the self-cleaning action of some leaf surfaces. Apart from lotus leaf, rose petal, several plant leaves, insect wings, water strider legs, Namib Desert beetle show superhydrophobic behaviour. Studies on several natural hydrophobic surfaces have shown that it exhibit hierarchical (micro/nanostructure) roughness **(Krishna et al., 2013).** If the leaf shows enough hydrophobicity, water will form near-spherical droplets that roll across the surface instead of sliding. Water droplets that hit the surface would quickly roll off, carrying dust and other particles with them. A super-hydrophobic surface repels water to such an extent that the contact angles obtained are extremely high; they are generally defined as surfaces with water contact angles above 150°. To form a surface with super-hydrophobic properties, a low-energy surface must be combined with high surface roughness **(Crick & Parkin, 2010)**.

Applications of self-cleaning coatings

Self-cleaning coatings has Potential application in sectors include;

- The textile industry (self - cleaning clothing)
- Automobile industry (self-cleaning windshield glass, car bodies and mirrors)

- Optical industry (cameras, sensors, lenses and telescopes)
- Marine industry (anticorrosion protection)
- Aerospace industry (non - sticky surfaces).

Self-cleaning coatings can also be used in windows (window coatings), solar modules (self-cleaning coatings for solar modules) and in paints (exterior paints with self-cleaning properties) **(Chem et al., 2011).**

1.7 Objectives

In this thesis, results and analysis aimed at proofing the potentiality of self – cleaning superhydrophilic and hydrophobic coatings against dust accumulation.

- To conduct a review on self – cleaning surfaces, types of self-cleaning coatings, and coating synthesis methods.
- To select suitable material for the fabrication of superhydrophilic and hydrophobic coatings.
- To fabricate the superhydrophilic and hydrophobic self –cleaning coatings accompanying properties of transparency.
- Optimization of coatings will be carried out by tuning the annealing temperature, concentration of the material for the achievement of synergistic properties such as transparency and WCA.

Chapter II

Review of Literature

CHAPTER - II

1. **(Z. He et al., 2022)** fabricated Si doped Tin Oxide thin-Film transistors by spin coating technique and the effects of Si doping concentrations on the properties of SnO_2 were explored. In this paper, TEOS is used as Si source. XRD patterns of Si doped tin oxide thin films with different Si concentrations shows that the obtained thin films are amorphous. When the Si concentration increases from 5% to 10% diffraction peaks occur at 26.63°, 33.83°, and 52.13° representing crystallinity. The oxygen vacancy was low as 16.69% for 2.5% Si doped SnO_2 film. The oxygen vacancy ratio and carrier concentration were concurrent with the change in Si concentration, which first decreased and then increased indicating that Si doping regulates the electrical properties of the film. Wettability studies showed that the contact angle of pure SnO_2 thin film and 10% Si doped thin films are 16.15° and 9.82° respectively. This shows that pure SnO_2 thin film is hydrophilic in nature and Si dopped thin film is super hydrophilic. Water Contact Angle less than 10◦, is applicable to self- cleaning application.

2. **(Daranfed, 2021)** analysed the effect of copper concentration on the structural, morphological, optical and electrical properties of Cu:SnO_2 thin films by using spray pyrolysis technique. XRD pattern confirmed that the thin film is polycrystalline with tetragonal structure of rutile type. UV-Visible analysis showed that the mean transmittance value is 71.27%. Doping copper with SnO_2 thin film increases the optical band gap. Through electrical studies it is found that decrease in electrical conductivity from 2.53 to 0.041 (Ω.cm)-1 for undoped films up to 3% cu doping but for 4% Cu doping there is increase in electrical conductivity equal to 1.81 (Ω.cm)-1. Water contact angle test showed that CA is maximum (79°) for 2 wt.% Cu doped films and decreased to 57° and 48° for 3 wt.% and 4 wt.% Cu doped films respectively. Doping copper at low concentration (≤ 2 wt.%) improves the transmission and above 2 wt.% to Cu improves the electrical conductivity of the SnO_2-based film produced by the spray pyrolysis technique.

3. **(Kiruthiga et al., 2022)** Investigated optical, structural, and electrical properties of transparent conductive Tin oxide thin films prepared by nebulized spray pyrolysis for photovoltaic applications. The XRD analysis concluded that the crystallinity is increased after annealing and confirmed the presence of polycrystalline nature of SnO_2

thin film. SEM morphological studies revealed that the grains are found to be octahedral like structure. The annealed SnO_2 thin film shows the clear polyhedral like structure. The grain size and stoichiometric of the prepared material increases when the molar concentration increases with annealing temperature. EDX studies shows the presence of required elements (Sn = 85.75 %& O = 11.31 %) and after annealing it shows the elimination of impurities. From the Hall Effect as well as optical studies it is proved that the annealed samples are showing better conductivity and wider band gap than non-annealed tin oxide thin film. FTIR analysis was used to compare the bending and stretching vibrations of the functional groups associated with the O-Sn-O bond for both annealed and nonannealed samples. The optical band gap values are increased from 3.71 eV to 3.75 eV for with and without annealing samples due to quantum confinement effect.

4. **(Rameshkumar et al., 2020**)prepared transparent nanofilms (SnO_2) using spin coating technique used for solar cell application and investigated the optical and electrical properties of SnO_2 thin film. FTIR analyzation confirmed stretching vibrational modes on plane between tin and oxygen which confirmed the presence of Tin Oxide. The thickness of Tin Oxide thin film is 151.9nm obtained by using Stylus Profilometer instrument. It is found that the thickness decreases with the increase in rotations per minute (rpm). UV-Visible Spectrum Analysis for tin oxide thin film showed that the Transmission is about ~80%. Deposited SnO_2 thin film is suitable for many optical devices such as transparent electrode, solar cell etc.

5. **(Maache et al., 2020)** prepared Transparent nanostructured tin oxide thin films in the glass substrates by spin coating technique with appropriate annealing conditions. SnO_2 thin films have been studied and deposition parameters have been optimized. TEM images confirmed that the film surface is formed homogeneously of nano-sized particles with dense microstructure. The X-ray diffraction pattern of the crystalline SnO_2 thin films revealed the existence of single-phase rutile type tetragonal crystal structure. UV- VIS spectra confirmed that the films exhibit a transmission of > 85 % in the visible region (380nm- 700nm). Deposited SnO_2 thin film is suitable for many optical devices such as solar cells, gas sensors, surface acoustic devices, transparent electrodes.

6. **(Gao et al., 2021)** investigated the improvement in dust removal performance of Sb dopped SnO_2–SiO_2 film by sol gel dipping method. SiO_2 sol was prepared using TEOS. XRD pattern of pure SiO_2 thin film has typical broad peak, which indicates that the pure SiO_2 film is amorphous. The XRD patterns of all the ATO-SiO_2 films correspond to the standard spectrum of SnO_2, and no new crystal phases, such as Sb_2O_3, Sb_2O_5, appeared. Sb doping concentration increases from 9 mol% to 15 mol%, the average grain size of the Antimony-Doped Tin Oxide-SiO_2 thin film first increases and subsequently decreases from 5.1 nm to 2.9 nm. UV VIS spectra showed that the transmittance of SnO_2–SiO_2 coated film in the visible region (380–780 nm) is 93.2% and Sb dopped SnO_2–SiO_2 film decreases from 86.3% to 82.7% due to the increase in the number of excitable electrons and the generation of lattice defects. Electrical properties studies of the film showed that square resistance first decreases and subsequently increases, whereas the dust removal performance first increases and subsequently decreases. Dust deposition experiment results shows that, at 90◦ tilt angle antimony doped tin oxide-SiO_2 and SnO_2–SiO_2 thin films shows 64% and 30% of dust removal performance respectively. Hence Antimony-Doped Tin Oxide-SiO_2 film has better dust removal performance than SnO_2–SiO_2 film.

7. **(Zhang et al., 2018)** pr**e**pared Zr-doped SnO_2 thin films by spin-coating technique and investigated the morphology, structure, optical properties and electrical properties. XRD pattern of Zr dopped SnO_2 thin film confirmed the tetragonal rutile structure. AFM images of 5 at.% doping of Zr in SnO_2 thin film shows that obtained thin film have uniform surface without cracks. Electrical studies showed that the tin oxide films with 1 at.% zirconium doping show the lowest resistivity (2.91×10^{-2} Ω cm) and high carrier concentration (4.39×1019 cm^{-3}) with mobility (4.90 cm^2 /Vs) via Hall effect measurement system. UV- VIS spectra analysis shows that the average transmittance of the tin oxide films is 96% in the visible region (380nm- 700nm) by incorporating 7% zirconium and it decreased to 92% for 10% Zr doping. The optical band gap of the prepared films varies from 3.88 eV to 3.95 eV by increasing zirconium concentration. Obtained thin films are widely used in optoelectronic devices such as solar cells, gas sensors, light-emitting diodes and smart windows.

8. **(Doyan et al., 2019)** investigated the Optical Properties of Indium Doped SnO_2 thin Films prepared by Sol-Gel Spin Coating Technique. The results of UV- VIS spectra showed that the thin film is increasing in transmittance from 75 - 96.6% at wavelengths 300 - 350 nm while increasing the doping percentage from 3.19- 4.32%. Increasing the percentage of doping decrease the energy gap, both in the direct energy gap (3.64 - 3.57 eV) and indirect energy gap (3.92 - 3.87 eV). The optical activation energy of the SnO_2 thin films decreased with increasing doping percentage from 2.91 - 2.35 eV. The results of this study indicated that SnO_2: In thin films has high transmittance and low energy gap and widely applicable in solar cells, touch screen and gas sensors.

9. **(Adedokun et al., 2019)** investigated the effect of Annealing Temperature on Structural, Optical and Electrical Properties of Spin Coated Tin Oxide thin Films for Solar Cells Application. X-ray diffraction pattern showed polycrystalline tetragonal-cassiterite structure. Annealing thin films for different temperature such as 300℃, 400℃, 500℃, 600℃ increases the grain size of SnO_2 thin films as 10.90, 12.83, 14.62, 16.15, 17.01 respectively. Optical transmittance spectra of the films showed considerable transparency (80%) in the visible region(380nm-700nm) and the transparency decreases with the decrease in annealing temperature. The optical studies revealed that increasing the annealing temperature decreased the energy band gap from 4.121eV to 4.106eV. Thus the prepared thin films are applicable to solar cell application.

10. (**Widati et al., 2019**) prepared SiO_2 /TiO_2 coated thin films which increases the surface roughness and hydrophobicity of methyltrimethoxysilane (MTMS) coated glass. The deposition of SiO_2, TiO_2, and MTMS were conducted using a layer- by- layer dip coating technique. XRD pattern of SiO_2 and TiO_2 coated thin film displayed a broad peak at 15-35° confirmed amorphous phase. AFM images confirmed the surface roughness values for SiO_2 / SiO_2 /MTMS, TiO_2/TiO_2/MTMS, and SiO_2 / TiO_2/MTMS were 67.7, 7.13, and 115 nm, respectively. Water contact angle test results showed that SiO_2 / TiO_2 /MTMS and TiO_2/MTMS/SiO_2 coated glass have 115.56°$\pm$1.01° and 95.62°$\pm$ 1.96° CA respectively. SiO_2 / TiO_2 /MTMS produced higher contact angle and stability than TiO_2 /SiO_2 /MTMS.

11. **(Paul & Purkayastha, 2017)** developed nano structured thin films of TiO_2, SnO_2, & SnO_2/TiO_2 and deposited on a glass substrate by sol-gel method. XRD analysis showed that for bilayer SnO_2/TiO_2 crystallite size is ~8.1nm in contrast to pure SnO_2 (~5.1 nm) film. XRD pattern confirms the presence of SnO_2/TiO_2 bilayer thin film, evident from the co-existence of the tetragonal SnO_2 and anatase TiO_2. Wettability studies revealed that water contact angle is 3.2°, 11.8°, 37.4° for SnO_2/TiO_2, SnO_2 and TiO_2 thin films respectively. Super-hydrophilic surface of SnO_2/TiO_2 thin film had extensive application in anti- fogging and self- cleaning application.

12. **(Purkayastha & Krishna, 2018**) developed Fe and Ni Doped SnO_2 thin films by spin coating technique. XRD analyzation confirmed the tetragonal phase structure of SnO_2 thin film. FE SEM characterization shows the decrease in particle size for Fe and Ni dopant. The average particle size was estimated about 9 nm for SnO_2 films which decreased to 6.86 nm and 6.49 nm for the Fe-SnO_2 and Ni-SnO_2 films respectively. WCA test confirmed the contact angle of pure SnO_2 thin film is 11.8° increased with doping (38.7° for Fe and 48.6◦ for Ni). Further modification with stearic acid also increases the water contact angle upto108° for pure SnO_2 thin film, 110° and 111° for Fe and Ni dopped SnO_2 thin films. The influence of doping on the wettability of SnO_2 thin films was also reported. EDX analysis confirmed the presence of both pure and doped SnO_2. Fe-SnO_2 and Ni-SnO_2 surfaces has a potential for self-cleaning applications and also photocatalytic activity.

13. **(Wang et al., 2017)** prepared SiO_2/TiO_2 and $SiO_2/SnO_2/SiO_2–SnO_2$ interference type antireflective coatings with homogeneous multilayers. Optical thin film design of a 6-layer SiO_2/TiO_2 and a tri-layer $SiO_2/SnO_2/SiO_2–SnO_2$ was investigated. XRD pattern shows that TiO_2 and SnO_2 crystallize in the form of anatase and rutile phase, respectively. All diffraction peaks can be indexed and no impurity phase can be identified and confirmed the crystallite size of 16.6nm and 9.9 nm for TiO_2 and SnO_2, respectively. The SEM images showed that Rice-like crystallites of 27 nm in width which are uniformly distributed in the TiO_2 thin films. In contrast, the SnO_2 thin films consist of spherical crystallites as fine as 10 nm. UV-VIS spectra showed the transmittance of 98.2% and 98.6% for SiO_2/TiO_2 and $SiO_2/SnO_2/SiO_2–SnO_2$ multilayered thin films respectively. The results obtained in this work demonstrate the

great advantage of combining design with sol-gel preparation for antireflective coatings.

14. **(Belhamri & Hamdadou, 2016)** studied the effect of solution Concentration on structural and optical properties of SnO_2 thin films synthesized by the spin coating technique. X ray diffraction spectra (XRD) showed that the films deposited at different concentrations (0.7 mol/l, 1 mol/l, 1.5 mol/l) are polycrystalline with a rutile type tetragonal structure. Crystallite sizes of the samples were found between 17 to 39.8 nm. Optical transmission spectra showed that the tin oxide thin films has transmission of 59 to 44% for different concentration in the visible region (400nm- 800nm). The experimental results suggest that the varying concentration has an effect on the structural and optical properties.

15. **(Sohn et al., 2016)** fabricated SnO_2 Doped SiO_2 thin Film by Facing Target Sputtering Process. UV- VIS spectra showed a transmittance over 85% in the visible range (380nm- 700nm). WCA test shows super hydrophilicity (6.5°) of SiO-SnO_2 thin film at deposition rate of 4.5 min and it increases when deposition rate increases, WCA value was 6.5° at 4.8 nm/min, 12° at 11.3 nm/min, and 15.9° at 15 nm/min. The Si doped SnO_2 (30:70 wt.%) film deposited with a high deposition rate of 15 nm/min resulted with a WCA of 60°. In conclusion, found that the hydrophilic surface strongly depends on the film deposition rate during the facing target sputtering process. Super hydrophilic nature of Si doped tin oxide thin films can be used in self- cleaning application.

16. **(Oluyamo & Agunbiade, 2016)** prepared Tin oxide thin film using automated spin coating technique and Investigated the surface morphology and optical characteristics of the deposited films. Optical characterization was done over a range of wavelength of 250 nm to 1000 nm which corresponds to photon energy between 1.2 eV to 5.0 eV. The average transmittance is 85 %, average optical conductivity is 0.032 x 1016 S^{-1}, average extinction coefficient is 1.25, average real dielectric constant is -7.5 and the band gap energy is estimated to be 3.78 eV. The SEM micrograph of the SnO_2 film shows the existence of some agglomerates of small rounded particles. Optical application of the tin oxide thin film includes anti- reflective coatings.

17. **(Lin et al., 2016)** investigated Structural and physical properties of tin oxide thin films prepared by RF magnetron sputtering technique for optoelectronic applications. X-ray diffraction pattern showed that a broad diffraction peak at ~23.6° indicating that the tin oxide films in this study are not amorphous hence XRD pattern confirmed that the SnO is orthorhombic structure and SnO_2 is tetragonal in structure. Water contact angle test showed that tin oxide films exhibit hydrophobicity because the water contact angles is above 90°, suggesting that the hydrophobicity was increased by reducing the sputtering pressure. Increasing the substrate temperature made the hydrophobic tin oxide films hydrophilic.

18. **(Sangchay, 2016)** prepared TiO_2 doped with SnO_2 thin film by sol-gel dip coating technique and investigated Phase transformation, surface morphology, photocatalytic and self-cleaning properties under fluorescent irradiation of thin films. XRD analyzation confirmed the presence of rutile phase in SnO_2 and anatase phase in TiO_2 at 1% mol concentration. Average crystallite size of TiO_2, TiO_2/ 1 SnO_2, TiO_2/2 SnO_2, TiO_2/3 SnO_2 thin films are 40.6, 15, 23.6, 33.1 Respectively. Scanning electron microscopic images showed cross sectional morphologies of TiO_2 doped with SnO_2 thin film and thickness range of 0.25 μm to 0.50 μm. Water contact angle test showed that 22.3° for the TiO_2 thin films, and 11.7°, 14.05°, 17.4° for the TiO_2/SnO_2 thin films with SnO_2 doping 1, 3 and 5 mol%, respectively. The result indicated that low doping of SnO_2 can improve the hydrophilicity of the TiO_2 thin films. TiO_2/SnO_2 thin films with doping SnO_2 1 mol% were found to exhibit the best photocatalytic activity and self-cleaning properties.

19. **(Yan et al., 2015)** proposed a fabrication of novel self-cleaning, super hydrophillic coating material based on double layer structure by using TEOS. FTIR image of Tetraethyl ortho silicate (TEOS)/ (2- acetoxy propyl) triethoxy silane (SIA) confirmed the existence of CH_3, CH_2, Si-o-Et, Si-O, C=O, C-O bonds. Contact angle for original glass and coated glass are measured as 52.15° and 4.7° respectively. Super hydrophilic property of such coatings could be used in PV cell glass surfaces, vechicle glasses and curtain walls.

20. **(Uysal & Arier, 2015)** investigated Structural and optical properties of SnO_2 nano films by spin-coating method. The XRD spectra of the SnO_2 thin films showed that the

formation of tetragonal rutile phase structure and confirmed that, increase in amount of water promotes the agglomeration which led to increase in the crystallite size. The obtained crystallite size of the prepared thin film is about 9 to 19 nm. AFM analysis showed that Surface roughness of SnO_2 films were determined to be 3.2, 4.3, 5.6, 6.9 nm (rms) for 1:0.0125, 1:0.025, 1:0.05, and 1:0.1 of SnCl2: water volume ratios, respectively. These quantitative findings in this work would be useful for the controlled synthesis and study of growth kinetics of SnO_2 nanoparticles and used for electronic and optical application.

21. (**Abdelkrim et al., 2016)** investigated effect of solution concentration on the structural, optical and electrical properties of SnO_2 thin films prepared by spray pyrolysis method. XRD studies indicated that the films are polycrystalline in nature with a tetragonal structure. Optical properties of SnO_2 thin films were investigated by UV–VIS spectra results shows that an average transmittance of the thin film is greater than 80% in the visible region (380nm-700nm) and high absorption (near 100%) in ultra violet region. The electrical properties of SnO_2 films were investigated by four-point probe method and it is found that the all samples have n-type conduction. Tin oxide thin films are used as transparent electrodes for photo electric conversion devices namely liquid crystal display, gas discharge display etc.

22. (Marikkannan et al., 2015) prepared tin oxide thin films from Tin Chloride dihydrate ($SnCl_2.2H_2O$) using different solvent by the sol-gel process for optoelectronic applications. The XRD peaks of the SnO-EtOH centred at $2\theta = 31.59^{\circ}$ corresponds to an orthorhombic (O) structure of SnO. It confirmed that the grain sizes of SnO-EtOH, SnO-IPA and SnO-MeOH films as 74 nm, 62 nm, and 94 nm, respectively. The UV-VIS spectra for spin coated tin oxide thin films showed that the samples have an optical average transmittance between 89 to 97% in the visible region (380nm- 700nm). The average transmittance in the visible region for the SnO-EtOH, SnO-IPA and SnO-MeOH samples were estimated to be 95%, 89%, and 97%, respectively. By analysing the optical properties of tin oxide thin films, it can be widely used in optoelectronic devices such as gas sensors, batteries, photo-catalysts, flat-panel displays, photoelectron chemical devices, and solar photovoltaic (PV) cells.

23. **(Shaban et al., 2015)** investigated and Studied the effect of a number of cycles on the structural and optical properties of SnO_2 thin films. XRD peaks showed that for 12 and 24 multilayer thin films are polycrystalline structure. SEM images of two different magnifications for the SnO_2 thin film deposited for 12 cycles showed many cracks. The crystallite size is increased from 7.7 to 31.1 nm as the number of deposition cycles increased from 12 to 24 cycle. UV- VIS spectra analyzation showed that the transmittances of these films are increased up to 65% for 24 cycle sample and up to 75% for 12 cycle sample in the region (400–1100 nm). SnO_2 thin films are widely used in gas sensors, solar cells, aerospace vehicles etc.

24. **(Shaban et al., 2015)** prepared Tin oxide thin film by the sol-gel method and investigated the effect of annealing temperature on multilayer film. SEM images for the SnO_2 thin films calcinated at 400℃, 500℃, 600℃, showed that the uniformity increases with increase in annealing temperatures. EDS spectrum of SnO_2 thin film confirmed that the oxygen content is twice that amount of tin, hence confirming the chemical composition to be SnO_2 and other impurities are not detected confirming high purity of the SnO_2 thin film. UV VIS characterization showed that increase in the annealing temperature decreases the transmission. Tin oxide thin films are widely used in gas sensing materials for gas sensor devices, aerospace vehicles.

25. **(Sangchay & Rattanakool, 2014)**investigated the effect of SnO_2 dopped with TiO_2 thin films on photocatalytic activity and hydrophilic property. Fabricated pure TiO_2 and SnO_2/TiO_2 thin films on glass substrate using a solgel dip coating technique. Strong diffraction peaks in XRD analyzation confirmed that high doping of SnO_2 into TiO_2 thin films can transform anatase phase to rutile and SnO_2 phase. The average crystallite size of SnO_2/TiO_2 thin films composed of various mol ratios of 0, 1, 3 and 5 mol% are 46.1, 20.7, 27.6 and 41.4 nm, respectively. SEM observations showed that thickness of pure TiO_2 and SnO_2/TiO_2 thin films are about 0.25-0.5 µm. WCA test under UV irradiation showed that for pure TiO_2 thin film is 27.7◦ and for 1, 3 and 5 mol% SnO_2 doped TiO_2 thin films are 14.4°, 21.2°, 28.3° respectively and confirmed that SnO_2 added in TiO_2 increases the hydrophilic property. 1 mol% SnO_2 doped TiO_2 thin films were found to exhibit photocatalytic activity and hydrophilic properties.

26. **(Mazloom & Ghodsi, 2013)** investigated influence of dopant concentration on structural, morphological and optical properties of thin films and prepared Cobalt doped SnO_2 thin films by sol–gel spin coating technique. XRD analyzation shows all samples have a tetragonal rutile structure and the grain size decreases with increasing the doping concentration. XPS results clearly showed the presence of Co_2+ ions into the SnO_2. The SEM and AFM images reveal that the morphology of samples was affected by dopant. The Hall effect results indicated that resistivity of films increased with Co doping. The optical band gap gradually decreases with improved cobalt concentration from 3.91 eV to 3.70 eV. The photo luminescence measurements reveals that decrease in intensity of blue emission and increase in green emission when content of Co is enhanced in thin films.

27. **(Ding et al., 2013)** investigated Electrical and optical properties of SnO_2 and N-doped SnO_2 thin films prepared by magnetron sputtering method by varying oxygen partial pressures from 0% to 3%. SEM images suggested that the nitrogen doping has a great influence on the growth and surface morphology of SnO_2 thin films. XRD pattern indicated that the nitrogen doping could not change the rutile structure when the oxygen partial pressure is below 3%. UV- VIS spectra results showed that the transmittance of SnO_2 thin films in the visible region (380nm- 700nm) decreased to around 80%, and the optical band gap decreased to about 3.6 eV when the oxygen partial pressure was 2%. But at the same time, the thickness increased from about 200 to 300 nm, which might also contribute to the decreasing of transmittance. For N: SnO_2 films, when the oxygen partial pressure was controlled from 0% to 1%, the average transmittance in the visible region was lower than that of un-doped films, which could be resulted from the double thickness. The results showed that the performance of SnO_2: N films was better than that of SnO_2 films and used in wide range of application such as solar cells, flat panel display etc.

28. **(Sakhare et al., 2013)** studied Structural, morphological, electrical and optical properties of Nanocrystalline SnO_2 thin films prepared by spin coating method. X-ray diffraction (XRD) analysis showed that SnO_2 thin films are crystallized in tetragonal structure rutile phase. Field emission scanning electron microscopy (FESEM) analysis revealed that surface morphology of the tin oxide thin film consists nanocrystalline grains with uniform coverage of the substrate surface. Transmission electron

microscopy (TEM) of SnO_2 thin film showed nanocrystals having diameter ranging from 5 to 10 nm. Selected area electron diffraction (SAED) pattern confirms tetragonal phase evolution of SnO_2. Atomic force microscopy (AFM) analysis showed surface morphology of Antimony doped SnO_2 thin film is smooth. Electrical properties of Antimony doped tin oxide thin films showed semiconducting nature with room temperature, electrical conductivity increases when processing temperature increases. Thermopower measurements confirms n-type conduction in Sb doped tin oxide thin films. It can be widely used in electronic and opto- electronic applications.

29. **(Ponomareva et al., 2012)** prepared Nanocomposite SiO_2-SnO_2 thin films on oxidized silicon substrates using sol-gel technique with tetraethyl orthosilicate (TEOS) as a silica source. AFM images confirmed that SiO_2-SnO_2 sample exhibits the
largest porosity with the average pore size of 10 nm and practically no porosity was observed in films prepared without addition of TEOS. Gas sensitivity of the samples was measured at different temperatures and for different H_2 concentrations. Sol-gel deposition of oxide layers exhibited advanced gas sensing properties which has wide application in Gas sensors.

30. (**Carvalho et al., 2012**) prepared SnO_2 thin films by dip-coating method and optical, electrical, structural properties are discussed. XPS analysis revealed stoichiometry of tin oxide thin films and very small quantities of chlorine and carbon as contaminants. The XRD pattern of tin oxide thin films confirmed that the obtained thin films are polycrystalline. EPS analyzation confirmed that the thickness of the film, which is approximately 100nm. The Conversion Electron Mossbauer Spectroscopy (CEMS) showed that SnO_2 is present in the film as single phase. The optical, electrical and structural properties of SnO_2 responsible for a large number of technological applications such as gas sensors, optical- electronic devices and displays.

31. **(Kirszensztejn et al., 2011)** synthesized series of SiO_2–SnO_2 samples with various Sn/Si molar ratios (0.05–1.0) by the sol–gel technique from (Tetraethyl orthosilicate) TEOS and Sn $(CH_3COO)4$ precursors in water free conditions. Created high surface area binary oxide gel (SiO_2- SnO_2) and studied the effect of tin component on the mesoporous structure. XRD pattern confirmed that the series of SiO_2–SnO_2 thin films of various molar ratio are in cassiterite phase. The low temperature nitrogen adsorption

measurements indicated the presence of both micro and mesopores. FTIR results showed the appearance of new IR bands at 1,048 and 882 cm-1, assigned to the stretching vibration of the three-dimensional Si–O–Sn network. The volume of the meso- and micropores in the systems with the tin component contribution not exceeding 20 wt%, was almost twice greater than that in the pure silica gel.

32. **(Serin et al., 2006)** investigated the effect of substrate temperature on the electrical, structural and optical properties of SnO_2 thin films prepared by spray pyrolysis method. X-ray diffraction studies showed that the crystallite size and preferential growth directions of the films were dependent on the substrate temperature and these studies also indicated that the films were amorphous at 300 ℃ and polycrystalline at 350 ℃. UV- VIS spectroscopic studies revealed that the optical transmittance in the visible region varied over the range of 75–95% with substrate temperature. It was observed that the films annealed at 400℃ maintain good electrical conductivity.

33. **(Manoj et al., 2007)** prepared indium doped tin oxide thin films by spray pyrolysis technique. X-ray diffraction studies have shown the polycrystalline nature of the films. Energy dispersive spectroscopy (EDS) studies revealed the presence of Sn, In and O from their characteristic X-rays. UV VIS spectroscopy studies shows that the transmittance improves from 79.5% to 84.8% with increasing indium concentration from 0.5 to 2 at.% respectively. Increasing indium concentration above 5% shows decrease in transmittance. SEM observations reveals the smooth surface morphology & crystallite size decreases from 15.9nm to 7.2nm with increasing indium doping. Obtained thin films are useful for gas sensing, as the sensitivity in gas detection improves with small grain size.

34. **(Gu et al., 2004)** prepared SnO_2 thin films on soda-lime glass substrate using a spin-coating method. XRD analyzation showed that the SnO_2 thin film has very poor crystalline nature and the diffraction lines are assigned well to tetragonal rutile crystalline phases. 3D AFM images showed that the SnO_2 thin films are uniform and crack-free, mainly consists of closely packed fine particles and the film surface is well crystallized and very smooth for the film calcined at 600℃ compared with the thin film calcined at 500℃. Optical studies confirmed the band gap of SnO_2 thin film is 4.38 eV.

Tin oxide thin films has wide range of applications in conductive electrodes, transparent coatings for heterojunction solar cells and chemical sensors.

35. **(Thangaraju, 2002)** studied Structural and electrical properties of highly conducting fluorine and antimony doped SnO_2 thin films from Stannic chloride by spray coating method. The deposition temperatures of SnO_2: F, SnO_2: Sb and SnO_2: (F+ Sb) thin films are 400℃, 350℃ and 375℃. XRD pattern confirmed that the obtained thin films are polycrystalline with a tetragonal crystal structure and the average grain size is approximately 300 A◦. It has been reported from the SEM micrograph analysis that the film morphology of $SnCl.2H_2O$ with HCl is similar to that obtained with $SnCl_4$. From the electrical studies it is concluded that the resistivities of the samples are of the order $10^{-3} – 10^{-4}$ Ω-cm. Fluorine doped samples are having lower mobility than the antimony and (F+ Sb) doped samples The transparent conducting metal oxide thin films are used as conducting solar window materials in thin film solar cells, heat reflectors for advanced glazing in solar applications and in various gas sensors.

Chapter – III

Materials and Methods

CHAPTER - III

3.1 Introduction

The materials and methods used to fabricate super hydrophilic and hydrophobic thin films for self- cleaning application are discussed in this chapter. Water contact angle (WCA) of thin film is the main parameter for self- cleaning application. Tendency of spreading sol over solid surfaces can be assessed by WCA. The materials were chosen depending upon their properties. These properties include adhesion, surface roughness and surface energy. Surface energy and surface roughness are two important specifications of surface that specify the WCA; higher surface energy leads to hydrophilicity and higher surface roughness leads to hydrophobicity **(Mohamad & Tilebon, 2022).** With low surface energy, less adhesion can be achieved between the liquid and solid interface, resulting in high surface roughness. By tuning the degree of surface roughness, transparency as well as self- cleaning ability of thin film can be achieved synergistically. Surface roughness can be controlled by coating parameters during the surface fabrication process.

3.2 Metal oxide

Metal oxides have been the subject of extensive research due to their wide range of applications in various fields, such as electronics, energy storage, catalysis, and sensing. Metal oxides are compounds formed by the combination of metal and oxygen atoms, where the metal atom acts as a cation and the oxygen atom as an anion. The properties of metal oxides depend on their composition, crystal structure, and size, and they can be tailored by controlling the synthesis conditions. Metal oxides have unique properties, such as high thermal stability, chemical inertness, and semiconductivity, which make them suitable for various applications. For example, metal oxide nanoparticles have been used in the development of solar cells, where they act as electron transporters, and in gas sensors, where they interact with gas molecules to produce a measurable electrical signal. Metal oxides offer several advantages over other materials, such as high energy density, low cost, and abundant availability. However, the performance of metal oxide-based materials can be improved by doping with other elements or by controlling their morphology.

3.2.1 Tin Oxide

SnO_2 belongs to the important family of oxide materials that combine low electrical resistance with optical transmission (>80%) in the visible range of the electromagnetic

spectrum. Although the SnO_2 is transparent in visible region, it is reflective in infrared region of light. This property is responsible for the use of SnO_2 as an energy conserving material. Generally, there are two main oxides of tin: stannic oxide (SnO2) and stannous oxide (SnO). The existence of these two oxides is attributed to the dual valency of tin with the oxidation states of +2 and +4 (**Sethi et al., 2015)**. Both of these oxides are known to be semiconducting materials with wide direct bandgap energy of 3.6 eV and indirect bandgap energy of 2.6 eV, where inherent oxygen vacancies act as an n type dopant **(Sun et al., 2017).** A unique feature of SnO_2 is the simultaneous occurrence of conductivity and transparency among the elements of group-IV in the periodic table. It crystallizes in rutile structure and can be synthesized in variety of shapes and size using different low cost synthesis techniques **(Bhagwat, 2015).** SnO_2 thin films has many advantages, such as economical, chemically stable, innoxious, mechanically stable, etc **(Zhang et al., 2018)**.

The properties of tin oxide can be controlled by various methods, such as doping, nanostructuring, surface modification etc. The incorporation of suitable dopants into the pure SnO_2 films causes a change in the microstructure of the films, which will cause changes in the electrical properties and other properties of the films.

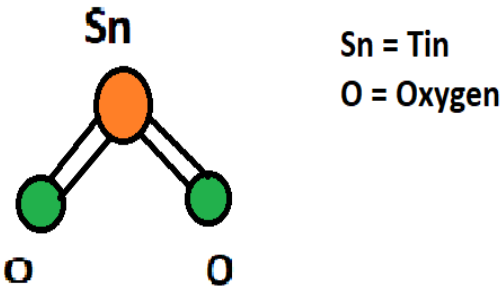

Fig 3.1 Structure of Tin Oxide

In the present work, preparation of SnO_2 thin films by sol–gel method achieved through the hydrolysis of inexpensive precursors, such as $SnCl_2$. Tin chloride dihydrate was used as the tin precursor, but it was modified through reaction with alcohol before hydrolysis **(Epifani et al., 2001).** Tin oxide films are stable at high temperatures, have excellent resistance to strong acids and bases at room temperature, resistant to mechanical wear, and have very good adhesion.

Applications

Unique properties of tin oxide such as high band gap, suitable optical characteristics and good structural resistance led to variety of applications such as;

- Gas sensors
- Low emission windows
- As electrodes in electroluminescent displays
- Imaging devices
- Antireflection coatings
- Transducers applications based on transparent conductors (e.g. window heaters for aircraft and cars, incandescent lamps, solar cells) and other optoelectronic devices **(Serin et al., 2006).**

3.3 Silane

Silane, also called **Silicon Hydride,** any of a series of covalently bonded compounds containing only the elements silicon and hydrogen, having the general formula Si_nH_{2n+2}, in which *n* equals 1, 2, 3, and so on. The silanes are structural analogues of the saturated hydrocarbons (alkanes) but are much less stable. Silanes are inorganic compound with chemical formula, SiH_4. Silanes are of practical interest as a precursor to elemental silicon. Silanes are used as coupling agents and well known for their property to modify the surface**.** The general formula for a silane has functionality hydrolysable groups X, organofunctional group R, silicon Si and a linker.

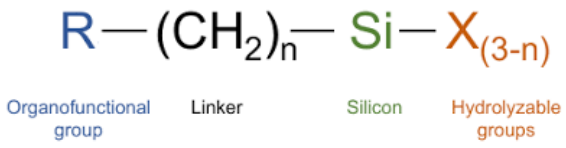

Fig 3.2 General formula for silane

3.3.1 TEOS

Tetraethyl orthosilicate commonly known as Tetraethoxysilane and abbreviated as TEOS, is the chemical compound with the formula $Si(OC_2H_5)_4$. TEOS is a colourless liquid that degrades in water. TEOS is the ethyl ester of orthosilicic acid, $Si(OH)_4$, it is prepared by alcoholysis of silicon tetrachloride.

$$SiCl_4 + 4\,EtOH \rightarrow Si(OEt)_4 + 4\,HCl \qquad \text{- - - - - - - - - - - (3.1)}$$

TEOS easily converts to silicon dioxide upon the addition of water:

$$Si(OC_2H_5)_4 + 2\,H_2O \rightarrow SiO_2 + 4\,C_2H_5OH \qquad \text{- - - - - - - - - - - (3.2)}$$

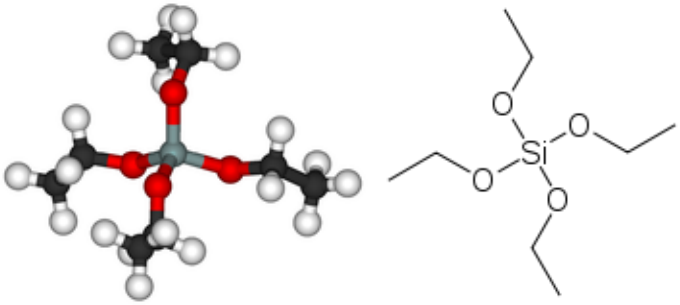

Fig 3.3 Structure of TEOS

Tetraethoxysilane is the main precursor material for the synthesis of zeolites and silicon dioxide, which is used in semiconductor industry. It is widely used as cross- linking agents in silicon polymers and in aerogel preparations. It is Stable, Flammable, Incompatible with strong oxidizing agents, water, alkalis, mineral acids.

Properties

a) Chemical formula : $(C_2H_5O)_4$ Si
b) Appearance : colourless liquid
c) Molecular weight : 208.329 g/mol
d) Density : 940 kg/m^3
e) Melting point : 196 K
f) Boiling point : 169 ℃
g) Structure : Tetrahedral molecular structure

3.3.2 MTMS

Trimethoxy(methyl)silane commonly known as Methyltrimethoxysilane abbreviated as MTMS, it is an organosilicon compound with general formula $CH_3Si(OCH_3)_3$. It is a crosslinker in the preparation of polysiloxane polymers. Methyltrimethoxysilane is tetrahedral and is often described as sp^3 hybridized. It has been used as a base in the formation of transparent sol-gel coatings on glass Substrates. Coatings on glass in order to modify its functional behaviours, Methyltrimethoxysilane used for instance because of its optical transparency, antibacterial property and self- cleaning behaviour **(Ismail et al., 2012)**. Methyltrimethoxysilane is usually prepared from Methyltrimethoxysilane and methanol. Alcoholysis of alkylchlorosilanes typically proceeds via an S_N2 mechanism. The combination of a low surface energy and a rough surface determines the hydrophobic properties. Methyl trimethoxysilane (MTMS) as an alkylsilane decreases the surface energy of a material. The hydrophobic properties are attributed to the methyl substituent of MTMS, while the methoxy group acts as a coupling agent forming the bonds with the substrate surface **(Widati et al., 2017).**

$$\mathbf{CH_3SiCl_3 + 3\ CH_3OH \rightarrow CH_3Si(OCH_3)_3 + 3\ HCl} \quad \text{- - - - - - - - -} \quad \mathbf{(3.3)}$$

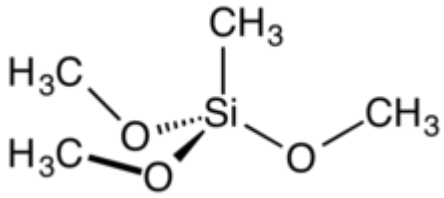

Fig 3.4 Structure of MTMS

Properties

a) IUPAC Name : Trimethoxy(methyl)silane
b) Chemical formula : $C_4H_{12}O_3Si$
c) Molar mass : 136.222 $g.mol^{-1}$
d) Appearance : Colourless liquid
e) Density : 0.955 g/cm^3
f) Boiling point : 104 ℃

3.4 Thin film technology

Thin film technology refers to the deposition of thin layers of material onto a substrate, typically with a thickness ranging from a few nanometers to several micrometers. Thin film technology has emerged as a crucial tool in various fields, including microelectronics, optics, etc. Thin film technology offers many advantages over bulk materials, such as improved surface properties, reduced material usage, enhanced performance, and cost-effective production.

Thin film deposition techniques can be broadly classified into physical and chemical methods. Physical methods involve the use of vacuum deposition techniques, such as sputtering, evaporation, and ion beam deposition, to deposit thin films onto a substrate. These techniques typically operate at high vacuum conditions and are well-suited for the deposition of metals, alloys, and ceramics. Chemical methods, on the other hand, rely on chemical reactions to deposit thin films. Examples of chemical deposition methods include sol-gel, chemical vapor deposition, and electroplating. These techniques offer high precision and control over the composition and morphology of the deposited thin films.

Application:

Thin film possesses attractive properties and therefore can have versatile applications.

- Devices with thin films occupy less space
- Their fabrication requires less material, hence inexpensive.

3.5 Sol gel Method

Sol-gel technology has emerged as an ideal fabrication method due to its low processing cost and its ability to control the morphology of the film **(Shaban et al., 2015).** The sol–gel process is a wet chemical technique, also referred to as chemical solution deposition which produces sol, that are dispersed and aggregated on the surfaces. The clustered particles subsequently afford high hierarchical rough surface. Surface roughness can be increased by etching, chemical grafting and the sol–gel process **(Widati et al., 2019)**. Among all the thin film methods, sol gel process offers a wide range of advantages over other methods such as low temperature processing, requires considerably less equipment and is potentially less expensive, easy coating of large surface, small thickness, high optical quality,

high purity. However, the most important advantage of sol-gel processing over conventional methods is the ability to control precisely the microstructure of the deposited thin film. i.e. volume, pore size, and surface area **(Latthe et al., 2019)**. The conventional sol-gel scheme involves continuous condensation of the particles formed initially due to the hydrolysis of the alkoxide precursor and finally forming gel which is commonly known as hydrolytic route.

Advantages

The sol-gel technique is predominantly advantageous for the development of thin coatings of oxides.

- Room temperature is the appropriate temperature for carrying out this procedure and the desirable morphology can be monitored by controlling the reaction conditions.
- Very small quantities of precursor are required and making the process economic, thus, the price of metal organic raw material is not of much significance.
- The sol-gel process maintains the option of synthesizing a large area and small area coating of thin oxide films at an economical technological applications. Many different industries are gaining profit from adopting solgel because of its flexibility in fabricating a wide range of materials with desirable characteristics.

3.6 Spin coating technique

Spin coating is widely used in micro-fabrication, where it can be used to create thin films thickness below 10 nm. It is used intensively in photolithography, to deposit layers of photoresist about 1 micrometre thickness. Spin coating is a procedure used to apply uniform thin films to flat substrates. A typical process involves depositing a small puddle of fluid resin onto the centre of a substrate and then spinning the substrate at high speed. Centrifugal force will cause the resin to spread to the edge of the substrate. Film thickness and other properties will depend on the nature of the resin (viscosity, drying rate, percent solids, surface tension, etc.) and the parameters chosen for the spin process. Spin coating technique is used in fabrication of thin films and manufacturing of integrated circuits, detectors, sensors, nanoscale devices etc.

3.6.1 spin coating process

There are four distinct stages to the spin coating process. These include:

- A dispense stage
- Substrate acceleration stage
- substrate spinning at a constant rate and fluid viscous forces dominate fluid thinning behaviour stage
- substrate spinning at a constant rate and solvent evaporation dominates the coating thinning behaviour stage.

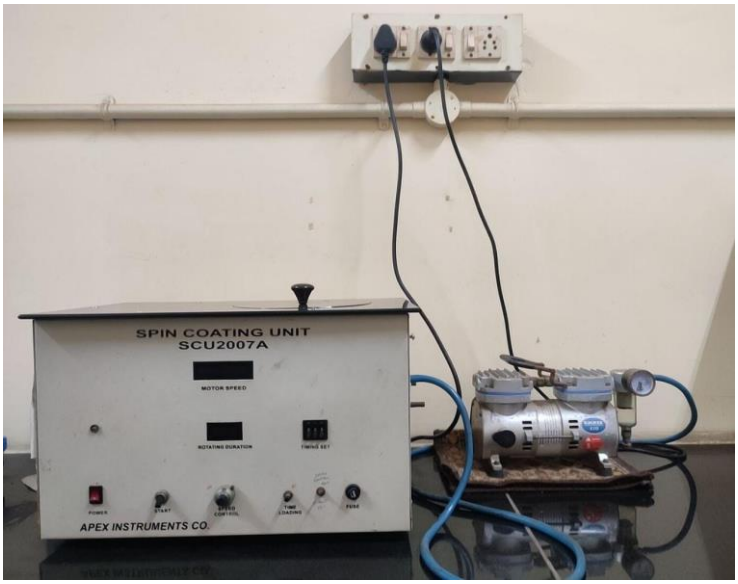

Fig 3.5 Spin coating unit (SCU2007A)

Advantages:

Spin coating technique is an attractive technique for thin film deposition for several reasons:

- It is low cost, less hazardous, and thus capable of easy scaling up, growth occurs at a relatively low temperature, compatible with flexible organic substrates
- It is a fast operating system.

- Film thickness is easily changed by changing spin speed, or switching to a different viscosity of sol **(Tyona, 2013).**
- Thin and uniform coating can be achieved at various thicknesses makes it ideal for both research and rapid prototyping.
- The ability to have high spin speeds leads to fast drying times (due to the high airflow) which in turn results in high consistency at both macroscopic and nano length scales, and often removes the need for post-deposition heat treatment.

Application:

- Spin coating technique is used in fabrication of thin films and manufacturing of integrated circuits, detectors, sensors, nanoscale devices etc.
- Single substrate spin processing is widely used in the semiconductor industry, where spin coating technique is used to create thin film less than 10nm thickness.

3.7 Experimental procedure for Thin Film Fabrication

SnO_2 metal oxide is dopped with TEOS & MTMS to fabricate super hydrophilic and hydrophobic thin films. The fabrication of thin film involves following steps,

- Substrate cleaning
- Solution preparation
- Spin coating deposition of solution onto the substrate

3.7.1 Substrate cleaning

Pre-cleaning removes water molecules, hydrocarbons and other contaminants from a substrate before thin film coating. The microscopic glass slide of dimension 2.5cm × 2.5cm were used as substrate for coating. Preliminarily, the substrates were soaked in extran solution for 45min followed by thorough water cleaning. And then soaked in HCl and deionized water for 45min. Finally, substrates were dried at 60℃ for an hour. Now the microscopic glass slides are ready for the deposition of thin films.

3.7.2 Synthesis of SnO_2 thin film

The solution is prepared using Tin chloride dihydrate ($SnCl_2 \cdot 2H_2O$) and ethanol in the molar ratio of 4.4317×10^{-4} M:0.08 M. The optimized amount of tin chloride dihydrate is weighed in the digital balance. The weighed quantity is added to a beaker containing ethanol and stirred for one hour at 30℃ in order to mix them **(Marikkannan et al., 2015).** Then transparent sol obtained was kept two hours at room temperature for aging. The condensed sol was deposited on the glass slide using a spin coating unit with the spinning speed of 2000 rpm for 30 seconds. The coated substrates were annealed at optimized temperature of 150 ◦C for one hour with a ramping rate of 5◦C/min.

3.7.3 Synthesis of SnO_2/TEOS thin film

The SnO_2/TEOS sol was prepared using 4.4317×10^{-4} M of $SnCl_2 \cdot 2H_2O$ and 2.23×10^{-3} M of TEOS. Initially, 0.08 M of ethanol was mixed with an appropriate ratio of water and HCl in a beaker by stirring for 5 min. Then an optimized amount of $SnCl_2 \cdot 2H_2O$ was added to it and stirred for 1 hour. After that, Tetraethoxysilane (TEOS) was slowly added to the solution drop by drop, and stirred continuously for 30min **(Wang et al., 2017)(Gao et al., 2021)** The transparent sol obtained was kept two hours at room temperature for aging and then used for deposition. The sol was deposited on the glass slide using a spin coating unit with a spinning speed of 2000 rpm for 90 seconds. The coated substrates were annealed at 250 ◦C for one hour with a ramping rate of 10◦C/min.

3.7.4 Synthesis of SnO_2/TEOS/MTMS thin film

The sol was prepared by mixing the precursor materials in the molar ratio SnO_2:TEOS:MTMS= 4.4317×10^{-4} M: 2.23×10^{-3} M:3.505×10^{-3} M. Initially, 0.08 M of ethanol was mixed with an appropriate ratio of water and HCl in a beaker by stirring for 5 min. Then an optimized amount of $SnCl_2 \cdot 2H_2O$ was dissolved to it and vigoursly stirred for 1 hour at 30℃. After that, Tetraethoxysilane (TEOS) was added to the solution slowly and stirred continuously for 30min. Finally, MTMS was slowly added to the solution drop by drop and stirred continuously for 30 minutues. The transparent sol obtained was kept 2 h at room temperature for aging and then used for deposition. The sol was deposited on the glass slide using a spin coating unit with a spinning speed of 2000 rpm for 90 seconds. The coated substrates were annealed at 250 ◦C for one hour with a ramping rate of 10◦C/min.

Chapter – IV

Results and Discussion

Chapter – IV

4.1 Introduction

In this chapter, characterization techniques, principles and interpretation of the results of all the samples have been explained. The presence of various functional groups are identified by Fourier transform infrared spectroscopy (FTIR). The X-ray diffraction (XRD) analysis is used in order to study the crystalline structure of the thin films and identify the preferred orientations of crystallites. The optical transmittance of the coating is measured using UV–Visible spectrometer. Wettability of the prepared samples are identified using Contact angle measurement. With 3D laser zeta profilometry the roughness of surface is analysed. Mechanical stability of the thin film is characterized using pencil hardness test.

4.2 Fourier transform infrared spectroscopy (FTIR)

Fourier transform infrared spectroscopy is a technique used to obtain a infrared spectrum of a absorption or emission of a solid, liquid or gas. FTIR spectrum consist of absorption peaks that corresponds to the frequencies of vibration between bonds of atom. FTIR technique is ideal for multilayer film characterization and particle analysis.

4.2.1 Principle and working

FTIR Spectroscopy, Fourier-transform infrared spectroscopy, is concerned with the vibration of molecules. Each functional group has its own discrete vibrational energy which can be used to identify a molecule through the combination of all of the functional groups. The FTIR machine consists of an infrared light source, an interferometer, a detector, and a sample holder. The infrared light source emits a beam of infrared radiation that is directed towards the interferometer. The interferometer splits the beam into two paths, one that is directed towards the sample holder and one that is directed towards a reference mirror. The sample holder contains the thin film to be analysed. As the infrared radiation passes through the thin film, it is absorbed by the atoms and molecules in the material. The detector then measures the intensity of the infrared radiation that has passed through the thin film. The interference between the two beams is used to generate an interferogram, which is then transformed into a spectrum using a Fourier transform algorithm. The resulting spectrum provides information about the chemical bonds and functional groups present in the thin film. FTIR spectroscopy is particularly useful for analysing organic and inorganic thin films. By analysing the peaks and bands in the FTIR spectrum, researchers can identify the chemical composition and structure of the thin film, as

well as any defects, impurities, or functional groups present in the material. Other features and options that may be included in an FTIR instrument include automated sample handling systems, attenuated total reflectance (ATR) accessories for the analysis of surfaces or powders, and specialized configurations for specific applications such as microscopy or imaging.

Fig 4.1 FTIR Spectrometer

4.2.2 Key components of FTIR

Source: A glowing black body emits the IR radiation. This radiation directed through an interferometer, where it is split into two beams by a beam splitter.

Interferometer: The interferometer is a critical component of an FTIR instrument. It is used to generate an interference pattern from the two beams of infrared radiation, which is then analysed to obtain a spectrum of the sample. The most commonly used interferometer is the Michelson interferometer, which consists of a fixed mirror and a moving mirror. As the moving mirror is scanned back and forth, the resulting interference pattern is converted into a spectrum of the sample.

Sample stage: The sample stage is where the sample to be analysed is mounted or placed. It is important that the sample is well-aligned and reproducible during the measurement to obtain accurate and reliable results.

Detector: The detector in an FTIR instrument is used to measure the intensity of infrared radiation transmitted through the sample. The most commonly used detectors are either single-element or multi-element detectors, such as a liquid nitrogen-cooled mercury cadmium telluride (MCT) detector or a room temperature deuterated triglycine sulfate (DTGS) detector.

4.3 X- ray diffraction (XRD)

X-ray diffraction (XRD) is a powerful non - destructive technique for characterizing crystalline materials. It provides information on structures, phases, preferred crystal orientations (texture), and other structural parameters, such as average grain size, crystallinity, strain, and crystal defects. X-ray diffraction peaks are produced by constructive interference of a monochromatic beam of X-rays scattered at specific angles from each set of lattice planes in a sample. The peak intensities are determined by the distribution of atoms within the lattice **(Andrei A. Bunaciu et al.,2015)**.

4.3.1 Principle and working

Based on the constructive interference of monochromatic x-rays and a crystalline sample in which the crystalline structure causes a beam of incident x-rays to diffract into many specific directions. The x-rays are generated by a cathode ray tube, filtered to produce monochromatic radiation, collimated to concentrate and directed toward the sample. Accelerating electrons with high voltages are allowed to collide with a metal target. If the bombarding electrons have sufficient energy, they can knock an electron out of an inner shell of the target metal atoms. Then the electrons from the higher states drop down to fill the vacancy, emitting x-ray photons with precise energies determined by the electron energy levels. These rays are called characteristic x-rays. Bragg's equation is used for measuring the angle of diffraction. The law states that when an x-ray is an incident onto a crystal surface, with an angle of incidence θ, it will reflect with the same angle of scattering θ.

$$n\lambda = 2d \sin\theta \qquad \text{- - - - - - - - -(4.1)}$$

Where, λ denotes beam wavelength, θ denotes angle of incidence, n is an integer and d denotes spacing between the plane. The XRD machine works by analysing the interaction of X-rays with the atoms in the thin film, producing a diffraction pattern that provides information about the crystal structure, orientation, and phase of the material. The XRD machine typically consists of an X-ray source, a detector, and a sample holder.

Fig 4.2 PANalytical XRD instrument

The X-ray source emits a beam of X-rays that is directed towards the sample. As the X-rays interact with the atoms in the thin film, they are scattered in different directions. The scattered X-rays are then detected by the detector, which records the intensity and angle of each scattered beam. The diffraction pattern produced by the XRD machine provides information about the crystal structure of the thin film. The peaks in the pattern correspond to the angles at which the X-rays are scattered, and the intensity of the peaks corresponds to the amount of scattering at each angle. By analysing the position, shape, and intensity of the peaks, researchers can identify the crystal structure of the thin film, as well as any defects, impurities, or strains in the material. The XRD machine can also be used to analyse the orientation and phase of the thin film. By varying the angle and position of the sample holder, researchers can analyse the diffraction pattern at different orientations of the thin film. This allows them to determine the preferred orientation of the crystal structure, as well as any changes in the crystal structure or phase of the material.

4.4 UV-Visible Spectroscopy

UV-Visible spectroscopy is a powerful analytical technique widely used in many fields of science, including chemistry, biology, physics, and materials science. The technique involves the measurement of the transmittance of light in the ultraviolet and visible regions of the electromagnetic spectrum. In UV-Visible spectroscopy, a sample is irradiated with light of a specific wavelength, and the intensity of the light transmitted through the sample is measured. The difference in the intensities of the incident and transmitted light is used to calculate the absorbance and transmittance of the sample at that wavelength.

4.4.1 Principle and working

The basic principle of UV – VIS spectroscopy is based on the transmission and absorption of light (ranges from nm) by different chemical compounds. It is the interaction of ultra violet and visible light with matter. Every chemical compound has a particular or distinct spectrum as it only absorbs a specific wavelength of light(radiation). There are two types of UV –visible spectrometers, Single beam UV – visible spectrophotometers and Double beam UV – visible spectrophotometers.

In Single beam UV-visible spectrophotometers the incident light passing from the source enters monochromator then that incident monochromatic light moves through a slit. Then it passes through a sample solution, where some of the incident light is absorbed by the sample while other is transmitted. That transmitted light is detected by the detector. The detected light is amplified, recorded, and displayed on a readout device. Single beam UV - visible spectrometer comprises of Light source, lens, grating, wavelength selector, curvette, detector, recorder. The instrumentation of single and double beam spectrophotometer is almost same. The basic difference from Single beam UV – VIS spectrometer is, that the beam of incident light is passing simultaneously to the sample and reference cells. The incident light splits and directed towards both the reference and sample cuvette. The transmitted beam is detected by the detectors. A double beam UV – VIS spectrophotometer needs two detectors that detect electron ratio to measure or calculate absorbance in a sample test.

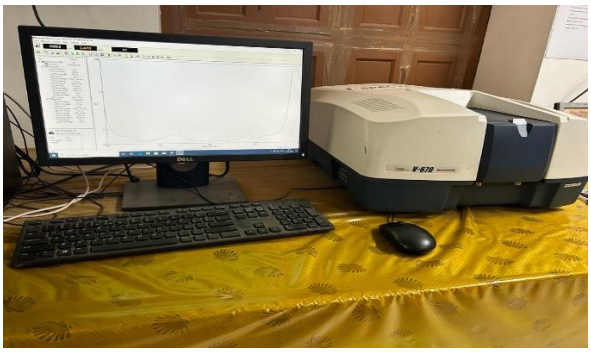

Fig 4.3 UV – VIS spectrophotometer (JASCO V-670)

4.4.2 Key components of UV – Visible spectrometer

Light source: Light sources that lie in the ultra violet and visible region are used as UV – visible spectrometer sources i,e., Hydrogen and deuterium lamps (Ranges 160-380nm), Xenon arc lamps (Ranges 250-600nm) and Tungsten halogen lamps (Ranges 240-2500nm).

Wavelength selector: Instrument with narrow bandwidth would be better for the functioning of UV – VIS spectrometer. Filters and Monochromators are two types of wavelength selectors.

Filters: Filters are used to permit a certain band of wavelength. Ultraviolet (UV) filters are optical filters which can be used to filter light in the ultraviolet part of the spectrum. These filters reduce haziness that can be created by the presence of ultraviolet light. The simplest type of filter is the absorption filter. Most commonly colored glass filters are used.

Monochromators: A monochromator is a mechanism that emits monochromatic light from a light source. A dispersive element, generally a prism or diffraction grating, is used to create the monochromatic light. A prism splits light into a spectrum by the fact, that the refractive index differs according to the wavelength when light passes through glass. A diffraction grating has parallel grating lines ruled on the surface. The serrated grating lines cause the reflected light to diffract and split into a spectrum. Major components of monochromator are slit, mirror, lens, grating/prism.

Sample holder: The sample can be placed in a quartz or plastic cuvette, depending on the solvent used and the path length required for the measurement.

Detector: The detector is used to measure the intensity of light that passes through the sample. The most common type of detector for UV-visible spectroscopy is a photodiode array detector, which can measure the entire spectrum at once. Other types of detectors, such as the photomultiplier tube (PMT), are also used in some applications. Additional instrumentation components that can enhance the performance of UV-Vis spectroscopy include a temperature controller, a reference cell, and a data acquisition system.

4.5 Water contact angle measurement

The contact angle is the angle formed between and the liquid droplet at the point of contact, and it provides valuable information about the surface properties of the material. The water contact angle is an important parameter that affects the wettability, adhesion, and surface energy of a material. Thin film measurements of water contact angle are used to investigate the surface properties of materials at the micro and nanoscale. These measurements are essential in understanding the behaviour of liquids on solid surfaces, which has significant implications in numerous applications, such as microfluidics, coatings, and biomaterials. The sessile drop method is a commonly used technique for measuring the surface wettability of solid substrates.

Fig 4.4 Contact angle measurement instrument

4.5.1 Principle and working

Contact angle measurement is a qualitative way to evaluate whether the surface has a hydrophobic or hydrophilic characteristic. It is based on the observation of the intermolecular interactions between the surface and a small drop of water when the drop meets the surface. It consists of a sample holder, a camera, and software for image analysis. The sample holder is designed to hold the material to be analysed in a horizontal position, with a flat surface facing up. To perform the water contact angle measurement, a small droplet of water is dispensed onto the surface of the material using a syringe or pipette. The droplet should be as small and uniform as possible to ensure accurate measurement of the contact angle. The droplet is allowed to equilibrate for a period of time, typically a few seconds, to ensure that it has fully spread out and made good contact with the surface. During this time, the camera records a high-resolution image of the droplet and the surface of the material. The image is then analysed using software designed to calculate the contact angle. The software identifies the edge of the droplet and the tangent to the droplet at the point of contact with the surface. The contact angle is then calculated based on the geometry of the droplet and the surface. Water contact angle measurement machines can be manual or automated. Automated machines can dispense and image droplets rapidly, allowing for high-throughput analysis of multiple samples. Some machines may also be equipped with environmental control chambers to vary the temperature and humidity during the experiment, allowing researchers to study the effects of these parameters on the wetting properties of the material.

4.5.2 Key components of water contact angle measurement

Camera and imaging system: They are used to capture an image of a sessile drop of water placed on the surface of the substrate, which is then analysed to determine the contact angle.

High-resolution cameras with high-speed imaging capabilities are typically used to obtain clear images of the droplet and substrate.

Dispenser: The dispenser is used to place a small droplet of water onto the surface of the substrate. This can be achieved using a syringe or other dispensing device, which must be capable of dispensing a precise volume of water to ensure consistent results.

Lighting system: The lighting system is used to illuminate the droplet and substrate to ensure clear imaging of the contact angle. The lighting must be uniform and bright enough to obtain clear images, while avoiding reflections and other optical artifacts.

Stage: The stage is where the substrate is placed for the water contact angle measurement. The stage should be stable and level to ensure accurate measurements.

4.6 3D laser profilometry

The 3D laser zeta profilometry is a powerful tool for characterizing surface topography and roughness of solid substrates with high precision and accuracy. The laser profilometry method is based on the processing of images of laser beams bent by the tested object profile. A surface profilometer uses high-precision data acquisition components to measure the distinct features of a product substrate on nano-, micro-, and macroscales. This is carried out through contact or non-contact methods.

4.6.1 Principle and Working

A 3D laser profilometer is an instrument that is used to measure the topography and surface roughness of a sample in three dimensions. The instrument works by using a laser beam to scan the surface of the sample and measuring the distance between the laser and the surface at each point. The laser profilometer consists of a laser source, a scanning mechanism, and a detector. The laser source emits a beam of light that is directed towards the sample, and the scanning mechanism moves the laser beam over the surface of the sample, typically in a raster pattern. As the laser beam scans the surface of the sample, it reflects back to the detector, which measures the time it takes for the light to return. By calculating the time delay, the distance between the laser and the surface at each point can be determined. The resulting data is processed by software to generate a 3D image of the surface of the sample. The image provides information about the height, depth, and shape of the surface features, as well as the surface roughness.

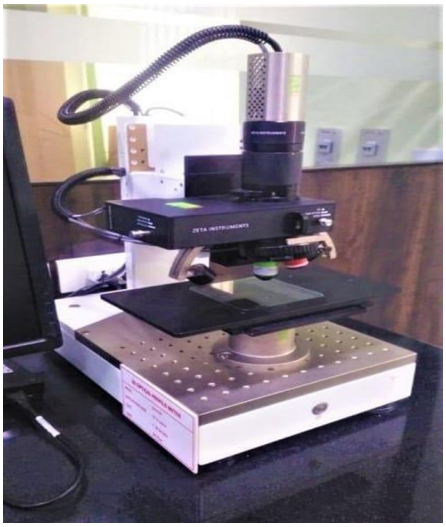

Fig 4.5 3D laser profilometer

4.6.2 Key components of 3D Laser Profilometry

Laser and optics system: The laser and optics system are critical components of a 3D laser zeta profilometry instrument. A laser is used to create a beam of light that is focused onto the surface of the substrate, and the reflection is detected by an array of detectors. The optics system is used to control the position and intensity of the laser beam, as well as to focus and direct the reflected light to the detectors.

Detector array: The detector array is used to detect the reflected light from the laser beam and convert it into a digital signal. The array must be capable of high-speed and high-resolution imaging to accurately capture the surface topography of the substrate.

Stage: The stage is where the substrate is placed for the 3D laser zeta profilometry measurement. The stage must be stable and level to ensure accurate measurements. The stage can be moved in three dimensions to allow for scanning of the entire surface of the substrate.

4.7 Durability study

Pencil Hardness Test

Scratch resistance of a coating is very essential as it deploying for real time application. Here in the present study, the scratch resistance of the coating was performed by using pencil hardness test as per ASTM standard D3363-05 using variety of hardness pencils graded from 9B-9H. This procedure involved holding the pencil tightly against the coated substrate while moving it over the sample, which was laid out on a horizontal surface at a 45° angle. A

microscopic image analyser was used to analyse the changes in the surface profile. Pictorial representation of pencil scratch test is shown in the Figure 4.6.

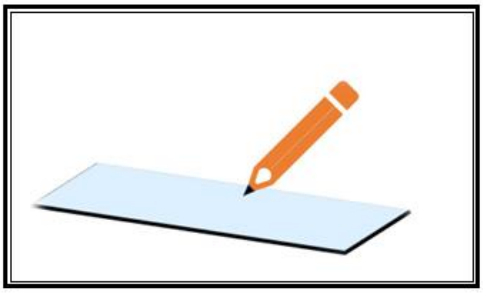

Figure 4.6 Pictorial representation of pencil scratch test

4.8 INTERPRETATION OF RESULTS

4.8.1 FTIR Analysis

Set - 1 SnO_2

The molecular vibration of the material was established using FTIR analysis. FTIR was used to determine the chemical bonding and functional groups in SnO_2 thin film in the wave number range of 500–4000 cm^{-1} shown in fig 4.7 (a). The peak near 3298 cm^{-1} is the stretching vibration of O-H **(Dong et al., 2021).** The peak at 1126 $cm^{-1}$is related to the vibration of hydroxyl-tin (Sn-OH) bond **(Selvi et al., 2014).** The band at 929 cm^{-1} refers to Sn – O stretching mode of Sn-O-Sn **(Blessi et al., 2014).** It can be seen that the vibrational bands at 823.6 cm^{-1} is attributed to the stretching vibrational modes in the plane between Tin (Sn) and Oxygen(O) like O-Sn-O **(Rameshkumar et al., 2020)**. The peak at 646 cm^{-1} and 709 cm^{-1} are the vibration of Sn-O-Sn and Sn-O in SnO_2 molecule **(Razeghizadeh et al., 2017)**. The peak at 578.64 cm^{-1} confirmed the formation of SnO_2 with characteristic vibrational mode of Sn–O **(Pusawale et al., 2011)**. The band appearing at 543 cm^{-1} is vibration of Sn-O **(Kirszensztejn et al., 2011).** The peak at 450 cm^{-1} are the stretching vibrations of O-Sn-O**.**

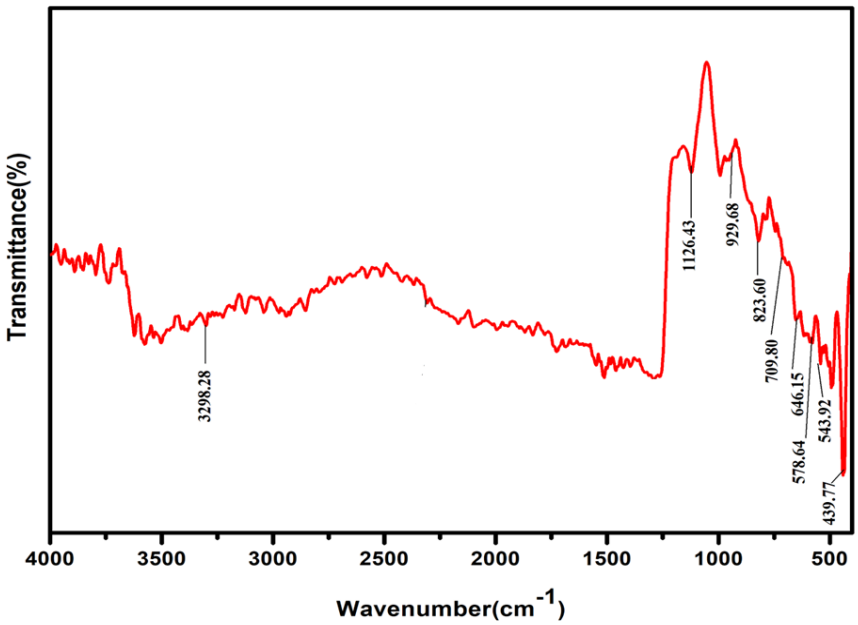

Figure 4.7 (a) FTIR spectra of prepared SnO_2 thin film

Table 4.1 FTIR peaks assignment of SnO_2 thin film

Peaks	Assignments
823, 439	Stretching vibration of O-Sn-O
578,543	characteristic vibration of Sn–O
646, 709	vibration of Sn-O-Sn and Sn-O
3298	stretching vibration of O-H
1126	Sn-OH bond
929	Sn – O stretching vibration

Set – 2 SnO_2/TEOS

The functional groups of SnO_2/TEOS thin film is elucidated by FTIR spectra are shown in the Fig 4.7 (b). Peak at 1168cm^{-1} represents the characteristic peak of -CH_3 (**Yan et al., 2015).** The peak appears at the wavenumber of 956 cm^{-1} , which is the Si-O- stretching mode of the Si-OH group **(Dong et al., 2021)**. It can be seen that the vibrational band at 815 cm^{-1} is attributed to the Si-O-Si bond. The band assigned to (Sn–O) appears at 624.94cm^{-1} in the spectrum of the sample. The peak at 555.50 cm^{-1} is due to the fundamental vibration of Sn-O

(Kirszensztejn et al., 2011). The band at 524.64 cm^{-1} is due to oxygen vibration in SnO_2 **(Sirohi et al., 2018).**

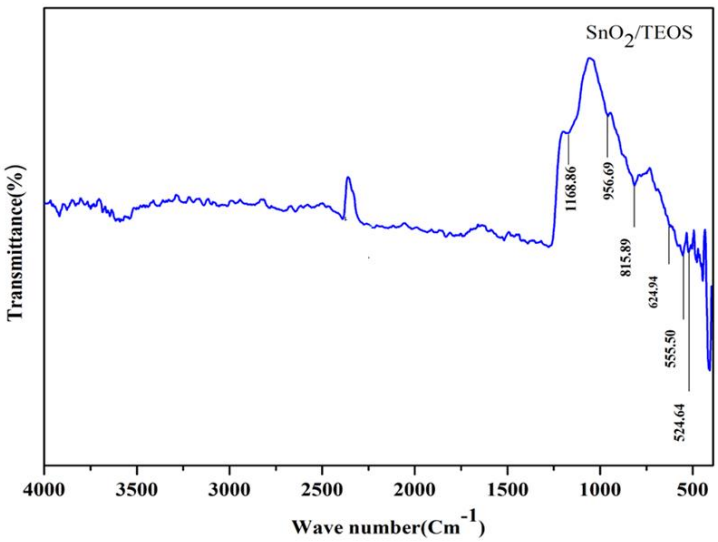

Figure 4.7 (b) FTIR spectra of prepared SnO_2/TEOS thin film

Table 4.2 FTIR peaks assignment of SnO_2/TEOS thin film

Peaks	Assignments
1168	characteristic peak of -CH_3
956	stretching vibration of Si-OH
815	stretching vibration of Si-O-Si bond
624	band assigned to Sn–O
555, 524	vibration of Sn– O

Set - 3 SnO_2/TEOS/MTMS

The figure 4.7 (c) shows FTIR spectra of SnO_2/TEOS/MTMS thin film. The absorption peak observed at 1263 cm^{-1} indicates the presence of the Si–CH_3 bonding **(Zhang et al., 2014).** The peak at 1120 cm^{-1} reveals the Sn-OH bond **(Selvi et al., 2014)**. The Si-O bond is shown by the peaks at 991cm^{-1} **(Yan et al., 2015).** It can be seen that the vibrational band at 819 cm^{-1} is attributed to the Si-O-Si bond. The 653.87 cm^{-1} peak assigned to (O–Sn–O) bond **(Kirszensztejn et al., 2011)**. The peak at at 578 cm^{-1} confirmed the formation of SnO_2 with characteristic vibrational mode of Sn–O **(Pusawale et al., 2011)**. The peak at 441 cm^{-1} are the

stretching vibrations of O-Sn-O**.** The symmetric stretching vibration of the Si-O-Si network and the bending mode is at the wave number of 435 cm^{-1} **(Dong et al., 2021).**

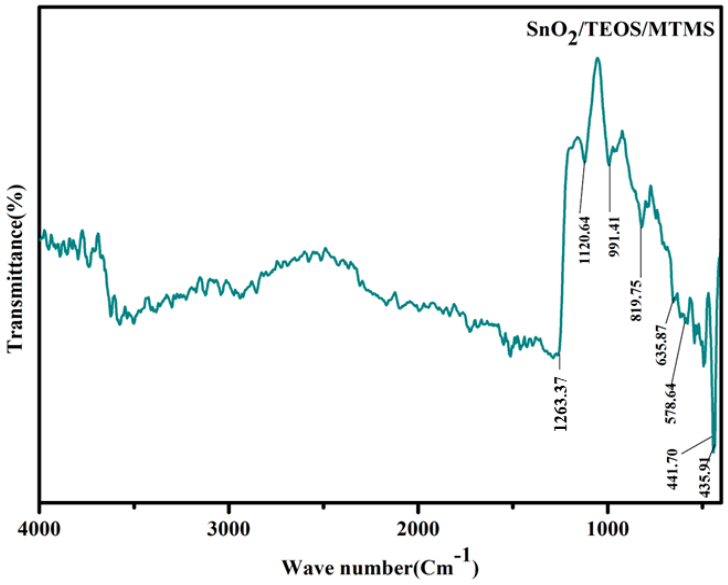

Figure 4.7 (c) FTIR spectra of prepared SnO_2/TEOS/MTMS thin film

Table 4.3 FTIR peaks assignment of SnO_2/TEOS/MTMS thin film

Peaks	Assignments
1263	Si–CH_3 bond
1120	Sn-OH bond
991	Si-O bond
819, 435	stretching vibrations of Si-O-Si bond
653,441	stretching vibrations O–Sn–O bond
578	characteristic vibration of Sn–O

4.8.2 XRD Analysis

Set - 1 SnO_2

The XRD pattern of the prepared SnO_2 thin film annealed at 150℃ is shown in Fig 4.8(a). The XRD measurements were recorded to analyse the structural parameters such as crystal structure, grain size, dislocation density, microstrain etc. The graph is plotted and the peaks are observed at (101), (211) and (301) miller planes. These values are compared with the Joint

Committee on the Powder Diffraction Spectra Data card number (JCPDS Card No). The prominent peak was observed at 2θ =32°.This peak corresponds to tetragonal phase of SnO_2 **(Varshney et al., 2020)**. They are indexed on the basis of (JCPDS data card No: 77-2296). Next the highest peak is present at 52.21° with (211) miller planes and at diffraction angle of 66.28° at (301) miller planes also the peak present. This confirms the presence of polycrystalline nature of SnO_2 and is matched with (JCPDS card No. 41–1445)**(Kiruthiga et al., 2022).** The grain size or crystallite size was calculated using the equation Debye Scherrer Formula. It depends upon the Full Width Half Maximum and the angle of the peak. The crystallite size of the prepared samples can be calculated using the formula.

$$D = K\lambda/\beta \, Cos\theta(nm) \qquad \text{- - - - - - -- - - - - - - - -} \quad (4.2)$$

where, D is Crystallite size (nm), K is Scherrer constant (0.9), λ is Wavelength of the X-ray source (nm), β is Full width at half maximum (FWHM) of the diffraction peak (radians) and θ is Bragg angle (degrees). The calculated average crystallite size of SnO_2 thin film is 37.64 nm.

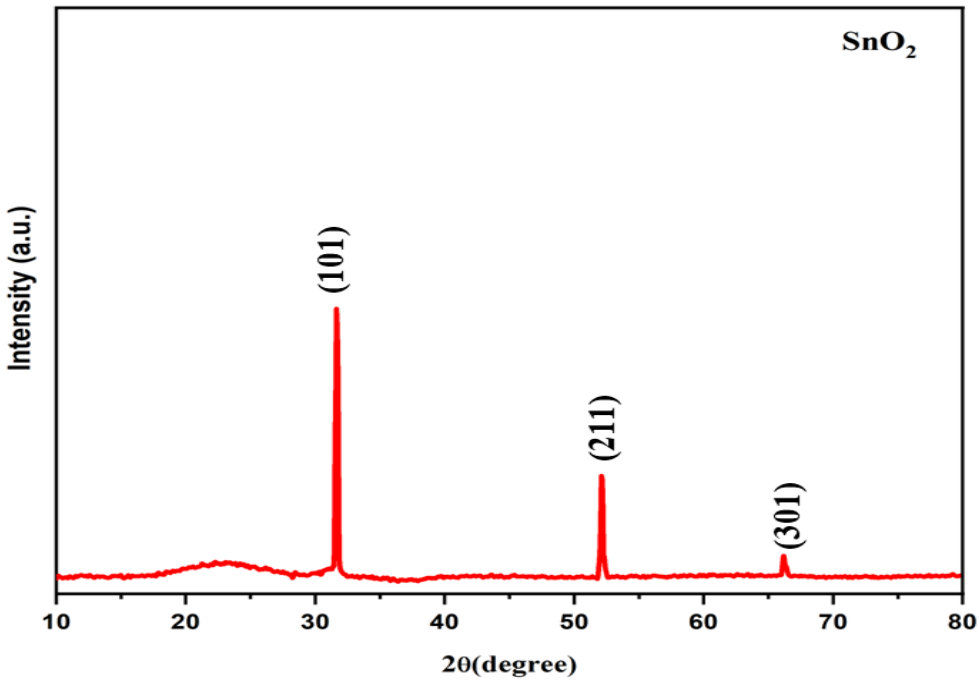

Fig 4.8 (a) XRD pattern of SnO_2 thin film

Set - 2 SnO_2 /TEOS

The XRD analysis of the SnO_2 /TEOS sample is shown in Figure 4.8 (b). The diffraction peak centered at 2θ = 32° corresponds to an tetragonal phase of SnO_2 **(Varshney et al., 2020)**. The peak located at 2θ=28° is corresponding to the diffractions of Si (111) plane **(Peng et al.,**

2015). The peak present at 52° with (211) miller planes confirms the presence of polycrystalline nature of SnO_2 and is matched with (JCPDS card No. 41–1445) **(Kiruthiga et al., 2022)**. The peak present at 2θ=24° indicates the presence of SiO_2**(Hariyanto et al., 2021).** Based on the values of FWHM, the average grain size of SnO_2/TEOS sample is estimated to be 20.2nm.

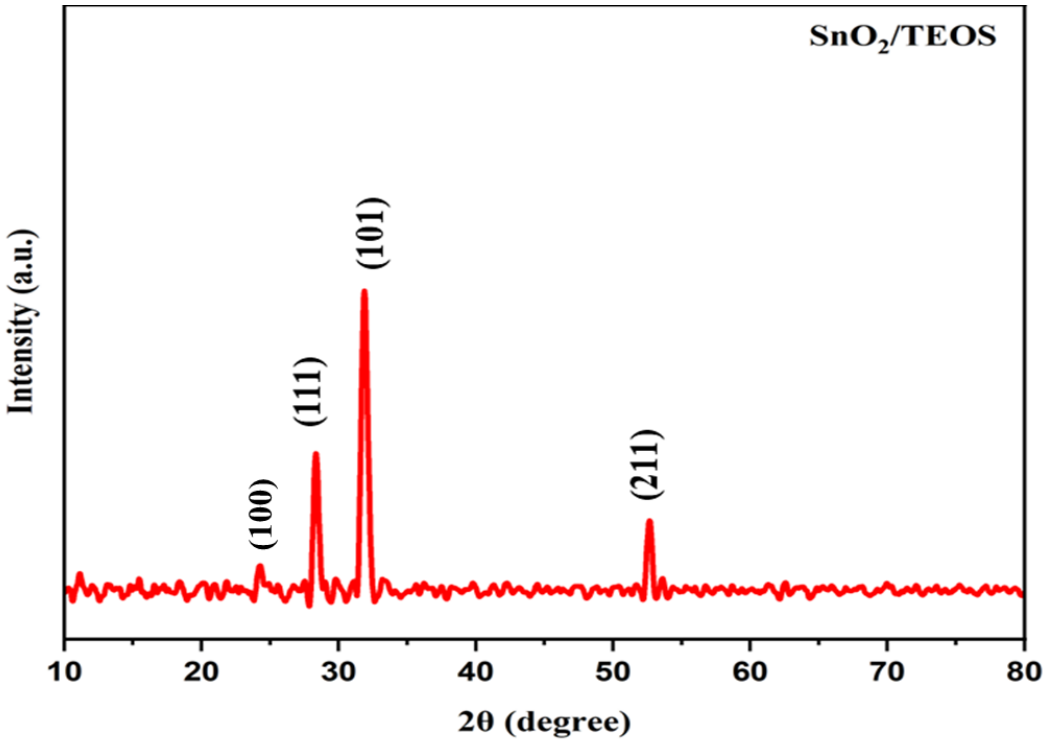

Fig 4.8 (b) XRD pattern of SnO_2/TEOS thin film

Set - 3 SnO_2 /TEOS/MTMS

The XRD analysis of the SnO_2 /TEOS/MTMS samples are shown in Figure 4.8 (c). The diffraction peak centered at 2θ = 32° corresponds to an tetragonal phase of SnO_2 **(Varshney et al., 2020)**. A peak present at 52.21° with (211) miller planes confirms the presence of polycrystalline nature of SnO_2 and is matched with (JCPDS card No. 41–1445) **(Kiruthiga et al., 2022)**. The peaks located at about 28° and 47° is corresponding to the diffractions from Si(111) and Si(220) planes respectively **(Peng et al., 2015).** The peak present at 61° represents the presence of SiO_2 **(Barati et al., 2019)**. The average grain size of SnO_2/TEOS/MTMS sample is 22.95 nm.

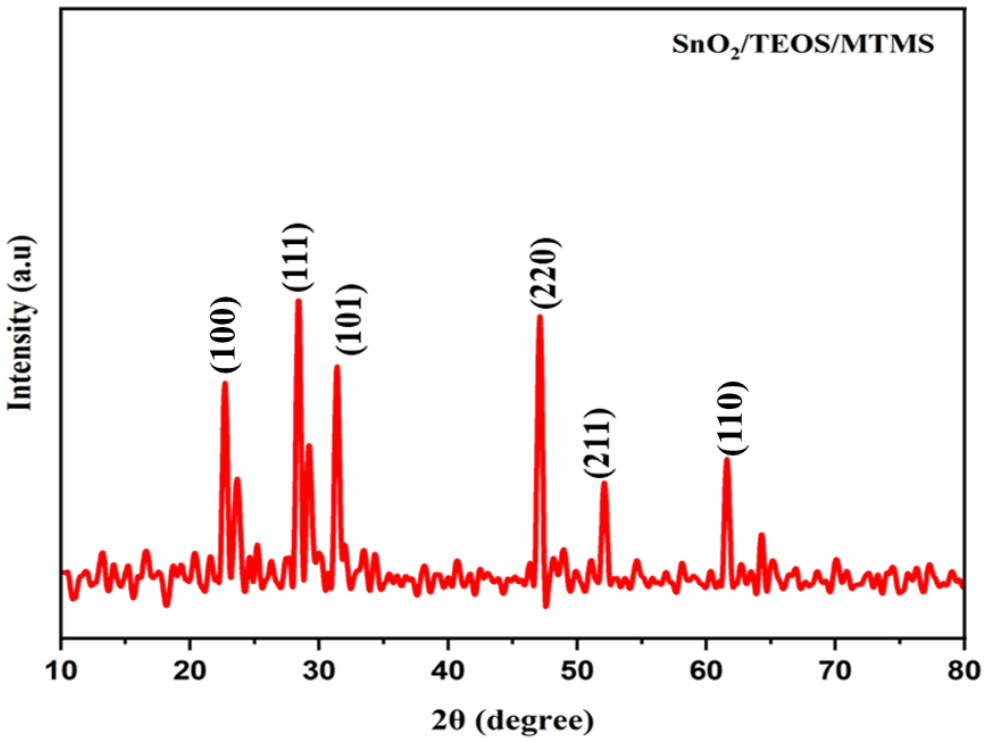

Fig 4.8 (c) XRD pattern of SnO_2/TEOS/MTMS thin film

4.8.3 Optical properties

Set – 1 SnO_2:

The optical transmittance spectra of Tin oxide thin film deposited on glass substrate is obtained by using UV-VIS spectroscopy technique. The annealing temperature of SnO_2 thin film is optimized at 150℃ to get better transmittance. As the annealing temperature increased, the transmittance of the SnO_2 thin film decreased. The SnO_2 thin film shows maximum transmittance of 88.06% at 598nm wavelength in visible region(300-1000nm) as shown in figure 4.9 (a), which is quite comparable with the reported values **(Rameshkumar et al., 2020)(Serin et al., 2006)(Maache et al., 2020)**. In this region of the spectrum (400 - 800 nm), the transmission is high which is due to the fact that there is no absorption and the reflectivity is low**(Belhamri & Hamdadou, 2016).**

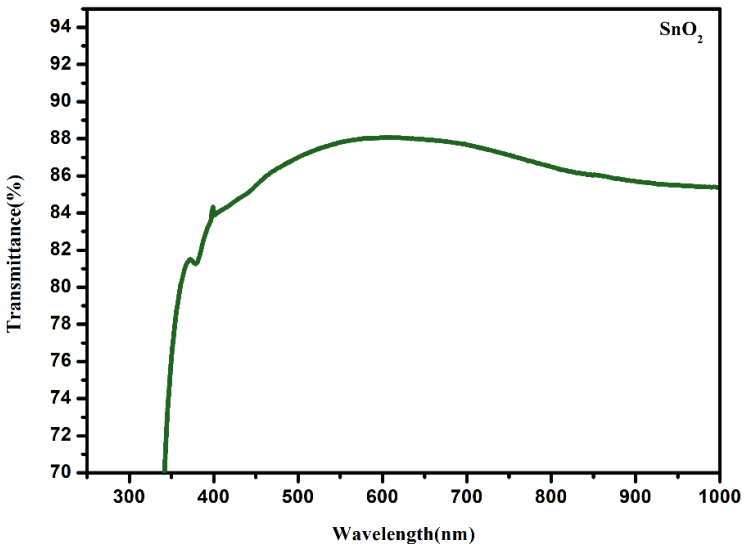

Figure 4.9 (a) Transmittance spectrum of SnO_2 thin films

Set – 2 SnO_2 /TEOS:

The transmittance spectrum of SnO_2/TEOS thin film is shown in Figure 4.9 (b). It exhibits maximum transmittance of 91% at 509 nm wavelength in the visible region (300-1000nm). It has been observed that TEOS increases the transmittance of SnO_2 thin film. Maximum transmittance was observed for SnO_2/TEOS sample annealed at 250℃.

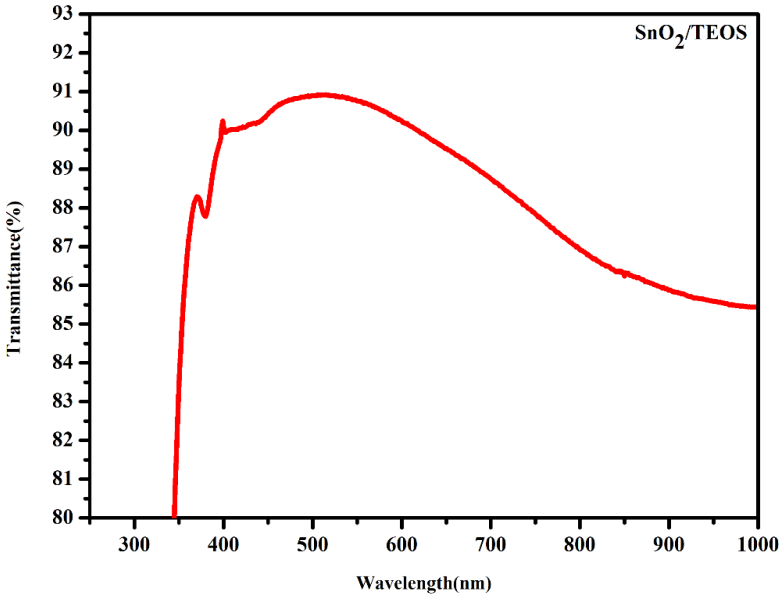

Figure 4.9 (b) Transmittance spectrum of SnO_2/TEOS thin film

Set - 3 SnO_2 /TEOS/MTMS

The transmittance of SnO_2/TEOS/MTMS sample was measured at visible region (300-1000nm). Maximum transmittance was observed at the sample annealed at 250℃. From figure 4.9 (c) it is observed that the microscopic glass slides has maximum transmittance of 90.4% whereas the SnO_2/TEOS/MTMS film shows the maximum transmittance of 93% at 553nm wavelength. Thus, the coating shows an increase of approximately 2% of maximum transmittance in the visible region as compared to bare glass. The hydrophobicity and transmittance are competitive properties from viewpoint of surface roughness. The roughness induces scattering of light and decreases intensity of transmitted light. In order to achieve higher transmittance of the coatings in the visible range (300-1000 nm), the surface roughness should be controlled below 100 nm or much higher than the certain range (more than few micro meters) **(Mahadik et al., 2010)**. Maximum transmittance and corresponding wavelengths are tabulated in table 4.4.

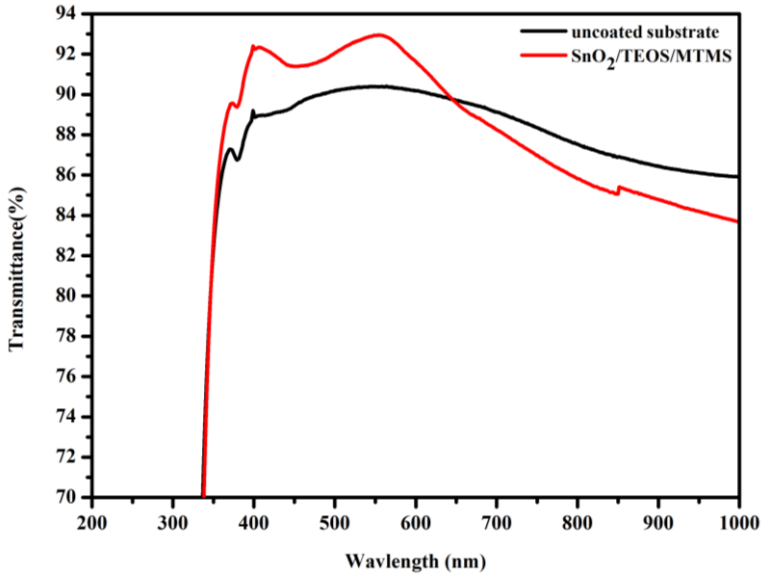

Figure 4.9 (c) Transmittance spectrum of uncoated substrate and SnO_2 /TEOS/MTMS coated substrate

Table 4.4 Maximum transmittance and corresponding wavelength for all three samples

Sample	Maximum Transmittance (%)	Wavelength(nm)
SnO_2	88.06	598
SnO_2 /TEOS	91	509
SnO_2/TEOS/MTMS	93	553

4.8.4 Thickness measurement

The gravimetric method is a commonly used technique for measuring the thickness of thin films. The method involves depositing the sol onto a substrate and then measuring the mass of the substrate with the deposited material. The thickness of the film can be calculated based on the mass and density of the material, as well as the area of the substrate. The difference in mass between the coated substrate and uncoated substrate gives the mass of the deposited film. The thickness of the film can be calculated using the following formula:

$$t = W/\rho A (nm) \quad \text{- - - - - - - - - - - - - - -} \quad (4.3)$$

where, W – weight of the deposition, ρ - density of the material, A- area of the coated region. The thickness is calculated and tabulated for SnO_2, SnO_2/TEOS and SnO_2/TEOS/MTMS thin films in Table 4.5.

Table 4.5 Experimental and Theoretical Thickness of the coated glass substrate of all three samples.

Sample	Experimental thickness (µm)	Theoretical Thickness (µm)
SnO_2	1.04	1.18
SnO_2 /TEOS	1.15	1.52
SnO_2/TEOS/MTMS	1.24	1.58

4.8.5 Wettability Analysis

Set – 1 SnO_2

The wettability of the films was tested by measuring the contact angle (θ) of a water droplet, placed on the film surface. SnO_2 thin film shows the water contact angle of 77.8°, clearly indicates that the obtained film has hydrophilic surface. The water contact angle usually depends on the surface roughness of the coated film. The theory was explained via Wenzel and Cassie-Baxter models. According to these models, the contact angle has a directly proportional relationship with surface roughness **(Swathi et al., 2021).** The surface roughness of the coating was measured using 3D laser zeta profilometry. Figure 4.10 (a) shows the 3D Laser profilometer image of SnO_2 thin film, the surface roughness of SnO_2 thin film is (Ra~0.37 µm). Figure 4.10 (b) shows histogram of SnO_2 thin film. The histogram image of SnO_2 thin film

shows the distribution of surface height of the sample, average height of SnO_2 thin film is ~ 25.4 μm.

(a)

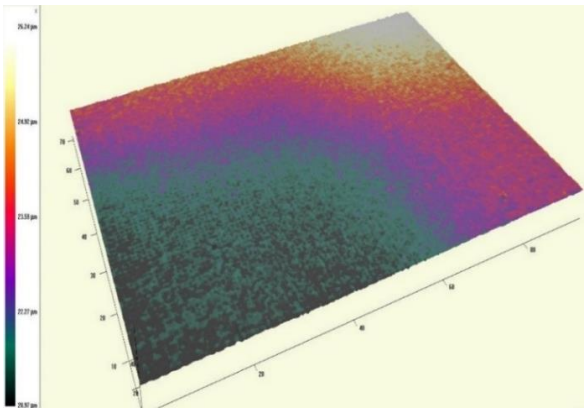

(b)

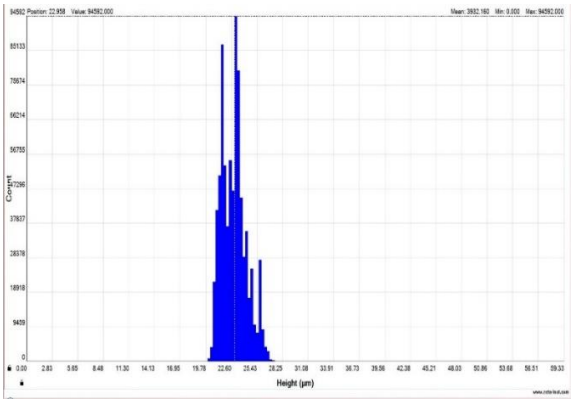

(c)

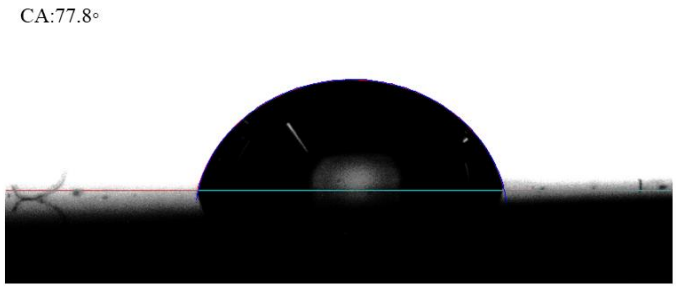

Fig.4.10 (a) 3D-Laser profilometer image of SnO_2 thin film (b) Histogram image of SnO_2 thin film and (c) Water contact angle of SnO_2 thin film

Set - 2 SnO_2/TEOS

Wettability of SnO_2 thin film enhanced by doping TEOS. From the figure 4.11 (a) and 4.11 (c), it was found that the film has average surface roughness (Ra~0.35 μm), with superhydrophilic contact angle of 10°. Doping TEOS in SnO_2 thin film decreases the WCA, since TEOS has hydrophilic nature. The hydroxyl groups present on the film surface are the main source of hydrophilicity as they promote the adsorption of water **(Rao et al., 2009)**. Figure 4.11 (b) shows histogram of SnO_2/TEOS thin film. The histogram image of SnO_2/TEOS thin film shows the distribution of surface heights of the sample, average height of SnO_2 thin film is ~ 85μm.

(a)

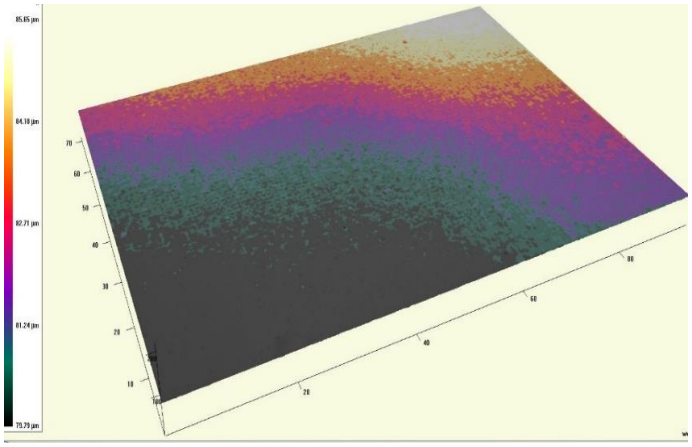

(b)

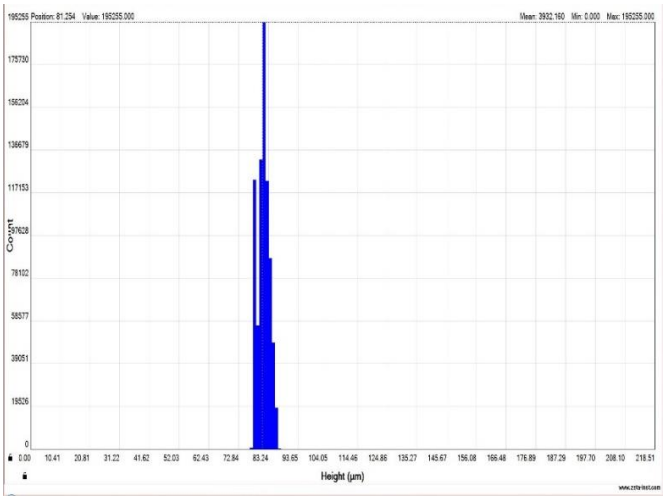

(c) CA =10◦

Fig 4.11 (a) 3D-Laser profilometer image of SnO_2/TEOS thin film (b)Histogram image of SnO_2 /TEOS thin film and (c) Water contact angle of SnO_2 /TEOS thin film

Set -3 SnO_2/TEOS/MTMS

Figure 4.12 (c) shows water contact angle of 94˚ which clearly indicates that the obtained thin film has hydrophobic surface. The non - wetting nature of the SnO_2/TEOS/MTMS thin film is attributed to the hydrophobic nature of MTMS **(Jacobs et al., 2021)(Rao et al., 2009)**. MTMS is known to create hydrophobicity by the replacement of Si–OH groups by hydrolytically stable Si-R (R = CH_3) groups, that inhibit the adsorption of water **(Jacobs et al., 2021)**. Figure 4.12 (a) and Fig 4.12 (b) shows 3D-Laser profilometer image of SnO_2/TEOS/MTMS thin film and histogram image of SnO_2/TEOS/MTMS thin film. The average height of SnO_2/TEOS/MTMS thin film is ~65.8 μm. The SnO_2/TEOS/MTMS film has increased surface roughness (Ra~0.53 μm). The wettability of a surface is determined by surface roughness and chemical composition **(Ardekani et al., 2019).** Average surface roughness, Root mean square roughness and Water contact angle of SnO_2, SnO_2 /TEOS and SnO_2/TEOS/MTMS thin film are tabulated in 4.7.

(a)

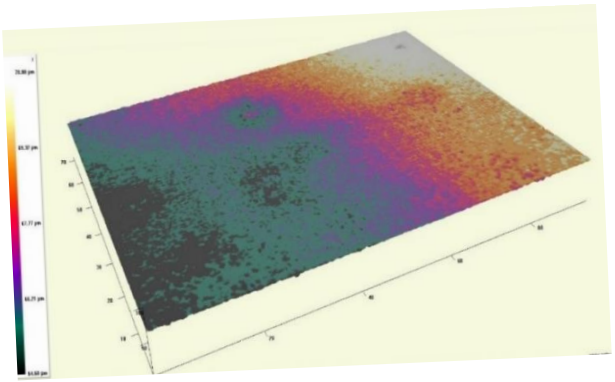

(b)

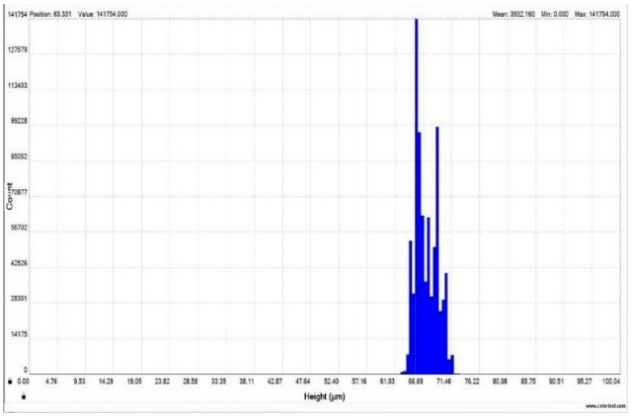

(c)

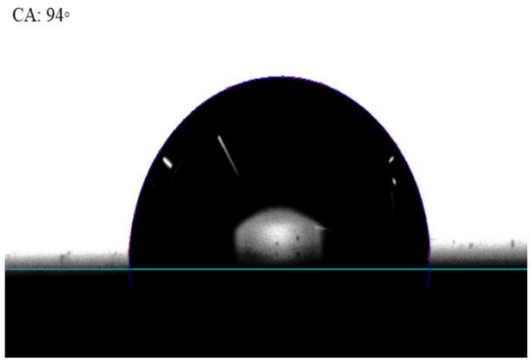

Figure 4.12 (a) 3D-Laser profilometer image of SnO_2/TEOS/MTMS thin film (b) Histogram image of SnO_2/TEOS/MTMS thin film and (c)Water contact angle of SnO_2/TEOS/MTMS thin film

Table 4.6 Average surface roughness, Root mean square roughness and Water contact angle of all three samples

Sample	Average surface roughness (µm)	Root mean square roughness (µm)	Water contact angle (Degree)
SnO_2	0.37	0.44	77.8
SnO_2 /TEOS	0.35	0.44	10
SnO_2/TEOS/MTMS	0.53	0.67	94

4.8.6 Mechanical stability

SnO_2/TEOS/MTMS

The scratch resistance of the prepared SnO_2/TEOS/MTMS sample was conducted by pencil scratching test as per the ASTM standard D3363-05 (American society for testing and materials 2010). Different hardness pencil graded from 9B-9H were used to perform scratch test. During testing the coated substrate was positioned at flat surface at 45° angle and the pencil was moved through it while being firmly held against it. SnO_2/TEOS/MTMS sample showed a scratch resistance against 3H hardness pencil and scratched by a 4H hardness pencil as shown in figure 4.13 (c). As surface roughness increases for SnO_2/TEOS/MTMS thin film, water contact angle being 94°, the prepared film exhibited scratch resistance against 3H hardness pencil.

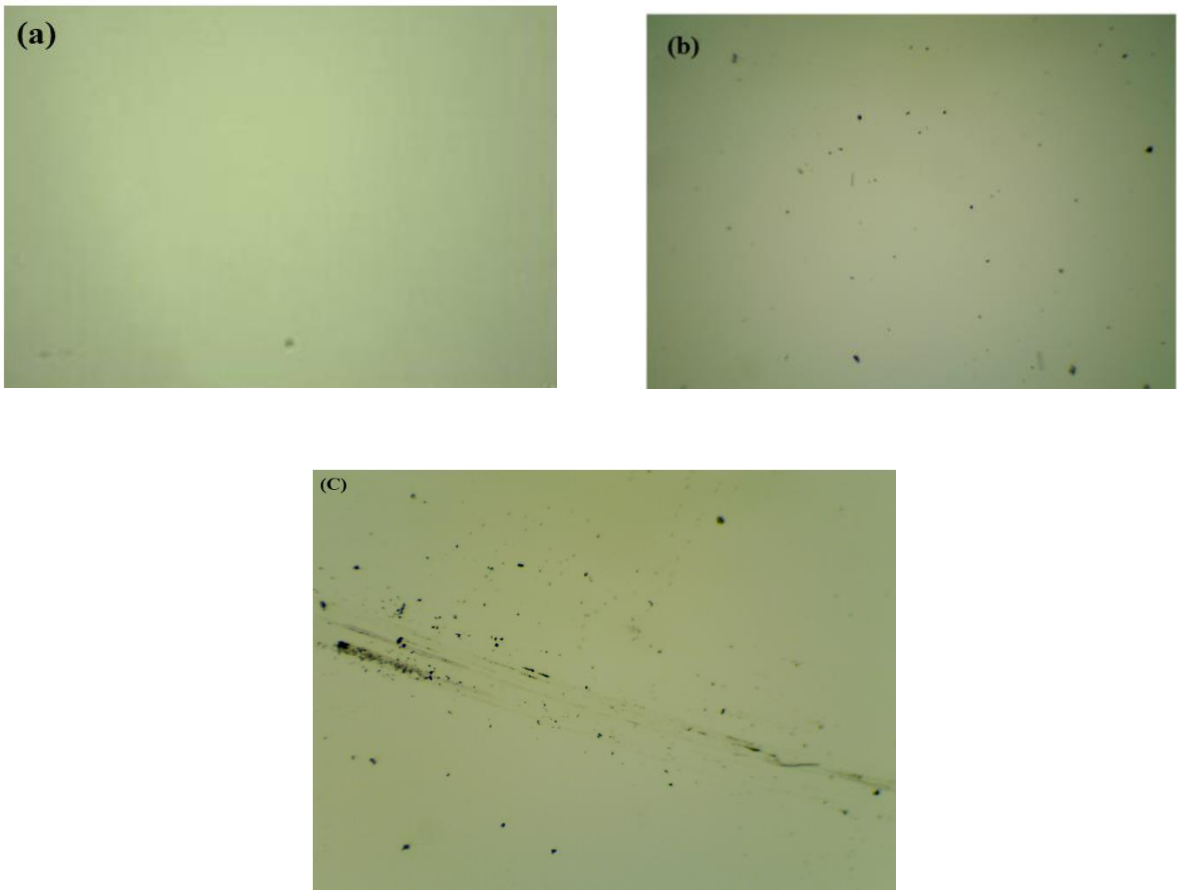

Figure 4.13 Optical image of SnO_2 /TEOS/MTMS sample (a)Before scratching (b)After scratching with 3H hardness pencil (c) After scratching with 4H hardness pencil

4.8.7 Application

Non wettability test on glass substrate

SnO_2/TEOS/MTMS coated substrate and uncoated substrate were tested for self - cleaning application. Dust particles were sprinkled on the substrate and water droplets were allowed to spread on it. Water spread out in uncoated substrate as shown in figure 4.14 (a). whereas, water droplets buckled up along with the dust particle in coated substrates. Coated substrate with the buckling of water is shown in figure 4.14 (b). Dust particles are sprinkled on coated and uncoated slides, few drops of water was allowed on the slides. Water spreaded along with the dust particles in uncoated substrate whereas, in the coated substrates the water gets clinged along with the dust particles making the surface dust free.

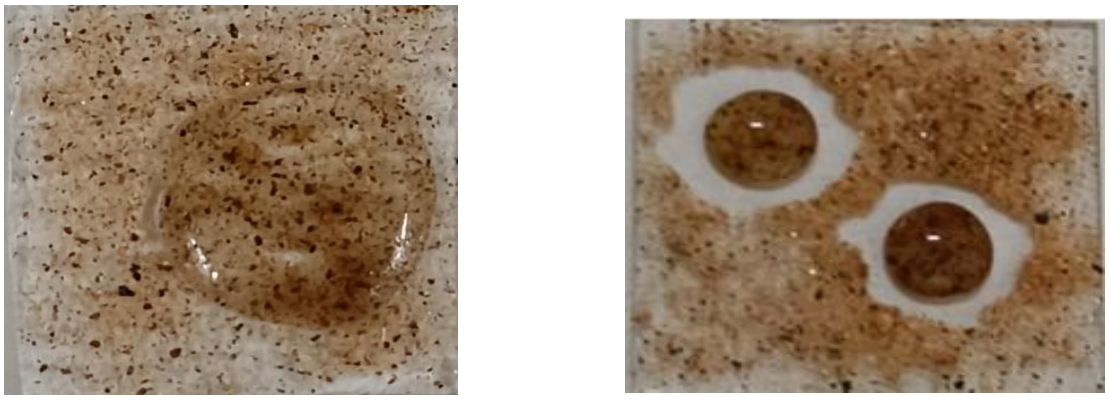

(a) **(b)**

Figure 4.14 (a) uncoated substrate (b) SnO_2/TEOS/MTMS coated substrate

Non-wettability test on cotton substrate

The cotton substrate were cleaned properly with acetone and immersed in SnO_2/TEOS/ MTMS for 10-15 minutes followed by drying in hot plate at 50℃ for 2 hours. The non - wettability of SnO_2/TEOS/MTMS coated and uncoated cotton substrate were tested using water, coffee, coke and milk drops gently deposited on the coated and uncoated cotton substrates with a standard single use syringe. The uncoated cotton surface fully absorbs water, coke, milk and coffee, while SnO_2/TEOS/MTMS coated cotton surface exhibits extreme non

wettable behavior for 3 hours. The visual image of coated and uncoated cotton surfaces towards water, coffee, coke and milk are shown in figure 4.15 (b).

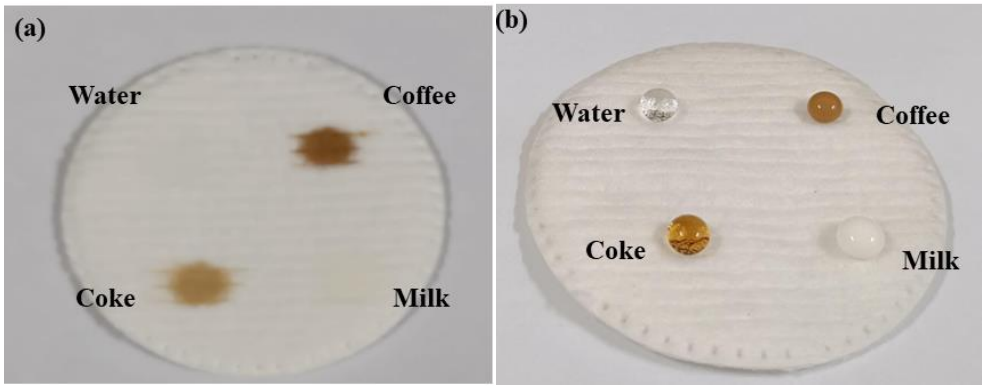

Figure 4.15 (a) uncoated cotton substrate towards water, coffee, coke and milk and (b) Coated cotton substrate towards water, coffee, coke and milk

Chapter – V

Summary and Conclusion

Chapter – V

Synthesis of SnO_2, SnO_2/TEOS and SnO_2/TEOS/MTMS thin films prepared by spin-coating technique has been analysed in this study. Explored the influence of silane dopants on the properties of the SnO_2 films. Prepared thin films are characterized by various techniques such as FTIR, XRD, UV – VIS spectroscopy, 3D Laser profilometry and WCA measurement. The self – cleaning ability of obtained SnO_2/TEOS/MTMS thin film on glass and non - wettability on cotton pad has been explored.

The characterization technique adopted for the prepared samples and the outcome of the results are summarized as below:

- Vibrational spectra of FTIR peaks showed O-Sn-O, Si-O bonds, and confirmed the presence of silane and SnO_2.
- The crystallite size of the prepared thin films were determined by XRD analysis.
- UV - Visible spectroscopy results showed highest transmittance of 93% SnO_2/TEOS /MTMS.
- 3D Laser profilometry results showed the average surface roughness of the obtained thin films.
- Mechanical stability of the prepared SnO_2/TEOS/MTMS thin film exhibited scratch resistance against 3H hardness pencil.
- Water contact angle analysis revealed the hydrophilic (77°) SnO_2, Superhydrophilic (10°) SnO_2/TEOS and Hydrophobic (94°) SnO_2/TEOS/MTMS nature of the prepared samples.

Chapter – VI

Bibliography

Reference

Abdelkrim, A., Rahmane, S., Abdelouahab, O., Abdelmalek, N., & Brahim, G. (2016). Effect of solution concentration on the structural, optical and electrical properties of SnO_2 thin films prepared by spray pyrolysis. *Optik*, *127*(5), 2653–2658. https://doi.org/10.1016/j.ijleo.2015.11.232

Adedokun, O., Odebunmi, V. M., & Sanusi, Y. K. (2019). Effect of annealing temperature on structural, optical and electrical properties of spin coated tin oxide thin films for solar cells application. *International Journal of Thin Film Science and Technology*, *8*(3), 157–162. https://doi.org/10.18576/ijtfst/080308

Aishwarya, S., Shanthi, J., & Swathi, R. (2019). Surface energy calculation using Hamaker's constant for polymer/silane hydrophobic thin films. *Materials Letters*, *253*, 409–411. https://doi.org/10.1016/j.matlet.2019.07.123

Ardekani, S. R., Rouh Aghdam, A. S., Nazari, M., Bayat, A., & Saievar-Iranizad, E. (2019). A new approach for preparation of semi-transparent superhydrophobic coatings by ultrasonic spray hydrolysis of methyltrimethoxysilane. *Progress in Organic Coatings*, *135*, 248–254. https://doi.org/10.1016/j.porgcoat.2019.05.033

Barati, F., Latifi, M., Far, E. M., Mosallanejad, M. H., & Saboori, A. (2019). Novel AM60-SiO_2 nanocomposite produced via ultrasound-assisted casting; production and characterization. *Materials*, *12*(23), 1-11. https://doi.org/10.3390/ma12233976

Belhamri, S., & Hamdadou, N. E. (2016). Concentration influence on structural and optical properties of SnO_2 thin films synthesized by the spin coating technique. *Journal of Physics: Conference Series*, *758*(1), 1-7. https://doi.org/10.1088/1742-6596/758/1/012007

Bhagwat, A. D., Sachin S. Sawant., Balaprasad G. Ankamwar., Chandrashekhar M. Mahajan., (2015). Synthesis of Nanostructured Tin Oxide (SnO_2) Powders and Thin Films Prepared by Sol-Gel Method. *Journal of Nano and Electronic Physics*, *7*(4), 7–10. http://essuir.sumdu.edu.ua/handle/123456789/43241

Blessi, S., Maria Lumina Sonia, M., Vijayalakshmi, S., & Pauline, S. (2014). Preparation and characterization of SnO_2 nanoparticles by hydrothermal method. *International Journal of ChemTech Research*, *6*(3), 2153–2155. https://sphinxsai.com/2014/vol6pt3/19/(2153-

2155)ICMCT14.pdf

Carvalho, D. H. Q., Schiavon, M. A., Raposo, M. T., De Paiva, R., Alves, J. L. A., Paniago, R. M., Speziali, N. L., Ferlauto, A. S., & Ardisson, J. D. (2012). Synthesis and characterization of SnO_2 thin films prepared by dip-coating method. *Physics Procedia*, *28*, 22–27. https://doi.org/10.1016/j.phpro.2012.03.664

Chem, J. M., Ganesh, V. A., Raut, H. K., Nair, A. S., & Ramakrishna, S. (2011). A review on self-cleaning coatings. *Journal of Materials Chemistry*, (21), 16304–16322. https://doi.org/10.1039/c1jm12523k

Crick, C. R., & Parkin, I. P. (2010). Preparation and characterisation of super-hydrophobic surfaces. *Chemistry - A European Journal*, *16*(12), 3568–3588. https://doi.org/10.1002/chem.200903335

Daranfed, W. Noubeil Guermat & Kamel Mirouh (2021). Analysis of the effect of copper concentration on the structural , morphological , optical and electrical properties of Cu : SnO_2 thin films.

Ding, X., Fang, F., & Jiang, J. (2013). Electrical and optical properties of N-doped SnO_2 thin fi lms prepared by magnetron sputtering. *Surface & Coatings Technology*, *231*, 67–70. https://doi.org/10.1016/j.surfcoat.2012.03.060

Dong, B., Gao, Y., & Liu, J. (2021). Preparation of SnO_2-SiO_2 film with high transmittance and strong dust-removing by sol-gel. *Optik*, *245*, 1–10. https://doi.org/10.1016/j.ijleo.2021.167727

Doyan, A., Susilawati, Hakim, S., Muliyadi, L., Taufik, M., & Nazarudin. (2019). The Effect of Indium Doped SnO_2 Thin Films on Optical Properties Prepared by Sol-Gel Spin Coating Technique. *Journal of Physics: Conference Series*, *1397*(1),1-9 https://doi.org/10.1088/1742-6596/1397/1/012005

Epifani, M., Alvisi, M., Mirenghi, L., Leo, G., Siciliano, P., & Vasanelli, L. (2001). Sol-Gel Processing and Characterization of Pure and Metal-Doped SnO_2 Thin Films. *Journal of the American Ceramic Society*, *84*(1), 48–54. https://doi.org/10.1111/j.1151-2916.2001.tb00606.x

Gao, Y., Liu, J., & Dong, B. (2021). Improvement of the dust removal performance of a high-transmittance SnO_2–SiO_2 film by Sb doping. *Ceramics International*, *47*(6), 8677–8684.

https://doi.org/10.1016/j.ceramint.2020.11.240

Gu, F., Wang, S. F., Lü, M. K., Cheng, X. F., Liu, S. W., Zhou, G. J., Xu, D., & Yuan, D. R. (2004). Luminescence of SnO_2 thin films prepared by spin-coating method. *Journal of Crystal Growth*, *262*(1–4), 182–185. https://doi.org/10.1016/j.jcrysgro.2003.10.028

Hariyanto, B., Wardani, D. A. P., Kurniawati, N., Har, N. P., Darmawan, N., & Irzaman. (2021). X-ray peak profile analysis of silica by Williamson–Hall and size-strain plot methods. *Journal of Physics: Conference Series, 2019*(1), 1-5. https://doi.org/10.1088/1742-6596/2019/1/012106

He, G., Zhou, C., & Li, Z. (2011). Review of self-cleaning method for solar cell array. *Procedia Engineering*, *16*, 640–645. https://doi.org/10.1016/j.proeng.2011.08.1135

He, Z., Zhang, X., Wei, X., Luo, D., Ning, H., Ye, Q., & Wu, R. (2022). Solution-Processed Silicon Doped Tin Oxide Thin Films and Thin-Film Transistors Based on Tetraethyl Orthosilicate. *Membranes 2022*, (12), 590-604. https://doi.org/ 10.3390/membranes12060590

Ismail, W. A., Ali, Z. A., & Puteh, R. (2012). Optical and physical properties of methyltrimethoxysilane transparent film incorporated with nanoparticles. *Advances in Materials Science and Engineering*, *2012*, 124820. https://doi.org/10.1155/2012/124820

Jacobs, M., De Vos, Y., & Middelkoop, V. (2021). Thickness controlled SiO_2/TiO_2 sol-gel coating by spraying. *Open Ceramics*, (6),1–7. https://doi.org/10.1016/j.oceram.2021.100121

Kirszensztejn, P., Kawałko, A., Tolińska, A., & Przekop, R. (2011). Synthesis of SiO_2-SnO_2 gels in water free conditions. *Journal of Porous Materials, 18*(2), 241–249. https://doi.org/10.1007/s10934-010-9376-2

Kiruthiga, G., Rajni, K. S., Geethanjali, N., Raguram, T., Nandhakumar, E., & Senthilkumar, N. (2022). SnO_2: Investigation of optical, structural, and electrical properties of transparent conductive oxide thin films prepared by nebulized spray pyrolysis for photovoltaic applications. *Inorganic Chemistry Communications, 145*, 109968. https://doi.org/10.1016/j.inoche.2022.109968

Krishna, M. G., Vinjanampati, M., & Purkayastha, D. D. (2013). Metal oxide thin films and nanostructures for self-cleaning applications: Current status and future prospects. *EPJ*

Applied Physics, *62*(3), 1-12. https://doi.org/10.1051/epjap/2013130048

Kung, C. H., Sow, P. K., Zahiri, B., & Mérida, W. (2019). Assessment and Interpretation of Surface Wettability Based on Sessile Droplet Contact Angle Measurement: Challenges and Opportunities. *Advanced Materials Interfaces*, *6*(18), 1–27. https://doi.org/10.1002/admi.201900839

Latthe, S. S., Sutar, R. S., Kodag, V. S., Bhosale, A. K., Kumar, A. M., Kumar Sadasivuni, K., Xing, R., & Liu, S. (2019). Self – cleaning superhydrophobic coatings: Potential industrial applications. *Progress in Organic Coatings*, *128*, 52–58. https://doi.org/10.1016/j.porgcoat.2018.12.008

Lin, S. S., Tsai, Y. S., & Bai, K. R. (2016). Structural and physical properties of tin oxide thin films for optoelectronic applications. *Applied Surface Science*, *380*, 203–209. https://doi.org/10.1016/j.apsusc.2016.01.188

Maache, M., Chala, A., & Devers, T. (2020). Characterization of spin coated tin oxide thin films for optoelectronic applications. *Journal of Nano- and Electronic Physics*, *12*(3), 1–5. https://doi.org/10.21272/jnep.12(3).03010

Mahadik, S. A., Kavale, M. S., Mukherjee, S. K., & Rao, A. V. (2010). Transparent superhydrophobic silica coatings on glass by sol-gel method. *Applied Surface Science*, *257*(2), 333–339. https://doi.org/10.1016/j.apsusc.2010.06.062

Manoj, P. K., Joseph, B., Vaidyan, V. K., & Amma, D. S. D. (2007). Preparation and characterization of indium-doped tin oxide thin films. *Ceramics International*, *33*(2), 273–278. https://doi.org/10.1016/j.ceramint.2005.09.016

Marikkannan, M., Vishnukanthan, V., Vijayshankar, A., Mayandi, J., & Pearce, J. M. (2015). A novel synthesis of tin oxide thin films by the sol-gel process for optoelectronic applications. *AIP Advances*, *5*(2). https://doi.org/10.1063/1.4909542

Mazloom, J., & Ghodsi, F. E. (2013). Spectroscopic, microscopic, and electrical characterization of nanostructured SnO_2:Co thin films prepared by sol-gel spin coating technique. *Materials Research Bulletin*, *48*(4), 1468–1476. https://doi.org/10.1016/j.materresbull.2012.12.069

Mohamad, S., & Tilebon, S. (2022). Anti-icing nano SnO_2 coated metallic surface wettability: optimization via statistical design. *Surfaces and Interfaces 21*,1-8.

http://doi/10.1016/j.surfin.2020.100720

Nakajima, A., Hashimoto, K., Watanabe, T., Takai, K., Yamauchi, G., & Fujishima, A. (2000). Transparent superhydrophobic thin films with self-cleaning properties. *Langmuir*, *16*(17), 7044–7047. https://doi.org/10.1021/la000155k

Oluyamo, S. S., & Agunbiade, D. B. (2016). Spin Coated Tin Oxide Thin Film For Optical And Optoelectronic Material Applications. *International journal of innovative Research and advanced studies*,3(8), 394-398. ISSN: 2394-4404

Parkin, I. P., & Palgrave, R. G. (2005). Self-cleaning coatings. *Journal of Materials Chemistry*, *15*(17), 1689–1695. https://doi.org/10.1039/b412803f

Paul, N., & Purkayastha, D. D. (2017). SnO_2/TiO_2 Bilayer Thin Films Exhibiting Superhydrophilic Properties. *AIP Conference Proceedings* 1832,1-4 https://doi.org/10.1063/1.4980495

Peng, S., Wang, D., Yang, F., Wang, Z., & Ma, F. (2015). Grown low-temperature microcrystalline silicon thin film by VHF PECVD for thin films solar cell. *Journal of Nanomaterials*, *2015*, 14–19. https://doi.org/10.1155/2015/327596

Ponomareva, A. A., Moshnikov, V. A., & Suchaneck, G. (2012). Mesoporous sol-gel deposited SiO_2-SnO_2 nanocomposite thin films. *IOP Conference Series: Materials Science and Engineering*, *30*(1),1-6. https://doi.org/10.1088/1757-899X/30/1/012003

Pratiwi, N., Zulhadjri, Arief, S., & Wellia, D. V. (2020). A Facile Preparation of Transparent Ultrahydrophobic Glass via TiO_2/Octadecyltrichlorosilane (ODTS) Coatings for Self-Cleaning Material. *ChemistrySelect*, *5*(4), 1450–1454. https://doi.org/10.1002/slct.201904153

Purkayastha, D. D., & Krishna, M. G. (2018). Dopant controlled photoinduced hydrophilicity and photocatalytic activity of SnO_2 thin films. *Applied Surface Science*, *447*, 724-731. https://doi.org/10.1016/j.apsusc.2018.04.028

Pusawale, S. N., Deshmukh, P. R., & Lokhande, C. D. (2011). Chemical synthesis and characterization of hydrous tin oxide (SnO_2:H_2O) thin films. *Bulletin of Materials Science*, *34*(6), 1179–1183. https://doi.org/10.1007/s12034-011-0168-3

Qian, X., Wang, N., Li, Y., Zhang, J., Xu, Z., & Long, Y. (2014). Bioinspired multifunctional vanadium dioxide: Improved thermochromism and hydrophobicity. *Langmuir*, *30*(35),

10766–10771. https://doi.org/10.1021/la502787q

Rameshkumar, C., Anderson, A., Ananth, D., Hinduja Mohan, T., & Subalakshmi, R. (2020). An investigation of SnO_2 nanofilm for solar cell application by spin coating technique. *Materials Today: Proceedings*, *45*, 6042–6045. https://doi.org/10.1016/j.matpr.2020.09.732

Rao, A. V., Latthe, S. S., Nadargi, D. Y., Hirashima, H., & Ganesan, V. (2009). Journal of Colloid and Interface Science Preparation of MTMS based transparent superhydrophobic silica films by sol – gel method. *Journal of Colloid and Interface Science*, *332*(2), 484–490. https://doi.org/10.1016/j.jcis.2009.01.012

Razeghizadeh, A. R., Zalaghi, L., Kazeminezhad, I., & Rafee, V. (2017). Growth and optical properties investigation of pure and Al-doped SnO_2 nanostructures by sol-gel method. *Iranian Journal of Chemistry and Chemical Engineering*, *36*(5), 1–8. https://doi.org/10.30492/ijcce.2017.23801

Sakhare, R. D., Khuspe, G. D., Navale, S. T., Mulik, R. N., Chougule, M. A., Pawar, R. C., Lee, C. S., Sen, S., & Patil, V. B. (2013). Nanocrystalline SnO_2 thin films: Structural, morphological, electrical transport and optical studies. *Journal of Alloys and Compounds*, *563*, 300–306. https://doi.org/10.1016/j.jallcom.2013.02.069

Sangchay, W. (2016). The Self-cleaning and Photocatalytic Properties of TiO_2 Doped with SnO_2 Thin Films Preparation by Sol-gel Method. *Energy Procedia*, *89*, 170–176. https://doi.org/10.1016/j.egypro.2016.05.023

Sangchay, W., & Rattanakool, T. (2014). Effect of SnO_2 addition into TiO_2 thin films on photocatalytic activity and hydrophilic property. *Advanced Materials Research*, *979*, 90–93. https://doi.org/10.4028/www.scientific.net/AMR.979.90

Selvi, N., Sankar, S., & Dinakaran, K. (2014). Interfacial effect on the structural and optical properties of pure SnO_2 and dual shells (ZnO; SiO_2) coated SnO_2 core-shell nanospheres for optoelectronic applications. *Superlattices and Microstructures*, *76*, 277–287. https://doi.org/10.1016/j.spmi.2014.10.015

Serin, T., Serin, N., Karadeniz, S., Sari, H., Tuğluoğlu, N., & Pakma, O. (2006). Electrical, structural and optical properties of SnO_2 thin films prepared by spray pyrolysis. *Journal of Non-Crystalline Solids*, *352*(3), 209–215.

https://doi.org/10.1016/j.jnoncrysol.2005.11.031

Sethi, R., Ahmad, S., Aziz, A., & Siddiqui, A. M. (2015). Structural, optical and electrical properties of tin oxide thin films for application as a wide band gap semiconductor. *AIP Conference Proceedings*, *1675*,1-6 https://doi.org/10.1063/1.4929255

Shaban, M., Attia, G. F., Basyooni, M. A., & Hamdy, H. (2015). Morphological and Structural Properties of spin coated Tin Oxide thin films. *International Journal of Engineering and Advanced Research Technology (IJEART)*, *1*(3), 11–14. http://www.ijeart.com/

Sirohi, K., Kumar, S., Singh, V., & Vohra, A. (2018). Synthesis and characterization of CdO-SnO_2 nanocomposites prepared by hydrothermal method. *Acta Metallurgica Sinica (English Letters)*, *31*(3), 254–262. https://doi.org/10.1007/s40195-017-0659-3

Sohn, S., Lee, C., Jung, S., & Kim, H. M. (2016). Hydrophilic surface of SnO_2 doped SiO_2 film by facing target sputtering process. *Journal of Nanoscience and Nanotechnology*, *16*(11), 11558–11562. https://doi.org/10.1166/jnn.2016.13551

Sun, Y., Zheng, J., Huang, R., Zhang, X., Chen, C., Jiang, B., Chen, H., Yan, L., & Yang, W. (2017). A simple method to control the microstructure and properties of sol-gel silica antireflective coatings. *RSC Advances*, *7*(51), 31950–31959. https://doi.org/10.1039/c7ra04400c

Swathi, R., Shanthi, J., & Anoop, K. K. (2021). Superhydrophilic TEOS/PF-127 based antireflection coating for solar and optical applications. *Optical Materials*, *118*,1-9 111246. https://doi.org/10.1016/j.optmat.2021.111246

Thangaraju, B. (2002). Structural and electrical studies on highly conducting spray deposited fluorine and antimony doped SnO_2 thin films from $SnCl_2$ precursor. *Thin Solid Films*, *402*(1–2), 71–78. https://doi.org/10.1016/S0040-6090(01)01667-4

Tyona, M. D. (2013). A theoritical study on spin coating technique. *Advances in Materials Research*, *2*(4), 195–208. https://doi.org/10.12989/amr.2013.2.4.195

Uysal, B.O., & Arier, U.O.A. (2015). Structural and optical properties of SnO_2 nano films by spin-coating method. *Applied Surface Science*, *350*, 74–78. https://doi.org/10.1016/j.apsusc.2015.04.023

Varshney, B., Siddiqui, M. J., Anwer, A. H., Khan, M. Z., Ahmed, F., Aljaafari, A., Hammud, H. H., & Azam, A. (2020). Synthesis of mesoporous SnO_2/NiO nanocomposite using

modified sol–gel method and its electrochemical performance as electrode material for supercapacitors. *Scientific Reports*, *10*(1), 1–13. https://doi.org/10.1038/s41598-020-67990-8

Wang, J., Ge, J., Hou, H., Wang, M., Liu, G., Qiao, G., & Wang, Y. (2017). Design and sol–gel preparation of SiO_2/TiO_2 and $SiO_2/SnO_2/SiO_2–SnO_2$ multilayer antireflective coatings. *Applied Surface Science*, *422*, 970–974. https://doi.org/10.1016/j.apsusc.2017.06.133

Widati, A. A., Nuryono, N., & Kartini, I. (2019). Design of SiO_2/TiO_2 that Synergistically Increases the Hydrophobicity of Methyltrimethoxysilane Coated Glass. *Open Chemistry*, *17*(1), 798–805. https://doi.org/10.1515/chem-2019-0087

Widati, A. A., Nuryono, N., Kartini, I., & Martino, N. D. (2017). Silica-methyltrimethoxysilane based hydrophobic coatings on a glass substrate. *Journal of Chemical Technology and Metallurgy*, *52*(6), 1123–1128. https://doi.org/10.1515/chem-2019-0087

Yamamoto, M., Nishikawa, N., Mayama, H., Nonomura, Y., Yokojima, S., Nakamura, S., & Uchida, K. (2015). Theoretical Explanation of the Lotus Effect: Superhydrophobic Property Changes by Removal of Nanostructures from the Surface of a Lotus Leaf. *Langmuir*, *31*(26), 7355–7363. https://doi.org/10.1021/acs.langmuir.5b00670

Yan, H., Yuanhao, W., & Hongxing, Y. (2015). TEOS/Silane-Coupling Agent Composed Double Layers Structure: A Novel Super-hydrophilic Surface. *Energy Procedia*, *75*, 349–354. https://doi.org/10.1016/j.egypro.2015.07.384

Zhang, X., Liu, X., Ning, H., Yuan, W., Deng, Y., Zhang, X., Wang, S., Wang, J., Yao, R., & Peng, J. (2018). Characterization studies of the structure and properties of Zr-doped SnO_2 thin films by spin-coating technique. *Superlattices and Microstructures*, *123*, 330-337. https://doi.org/10.1016/j.spmi.2018.09.016

Zhang, X., Zheng, F., Ye, L., Xiong, P., Yan, L., Yang, W., & Jiang, B. (2014). A one-pot sol-gel process to prepare a superhydrophobic and environment-resistant thin film from ORMOSIL nanoparticles. *RSC Advances*, *4*(19), 9838–9841. https://doi.org/10.1039/c3ra47185c